

The Effect of Stochasticity in Score-Based Diffusion Sampling: a KL Divergence Analysis

Bernardo P. Schaeffer^a, Ricardo M. S. Rosa^a, and Glauco Valle^a

^aInstituto de Matemática, Universidade Federal do Rio de Janeiro

July 31, 2025

Abstract

Sampling in score-based diffusion models can be performed by solving either a reverse-time stochastic differential equation (SDE) parameterized by an arbitrary time-dependent stochasticity parameter or a probability flow ODE, corresponding to the stochasticity parameter set to zero. In this work, we study the effect of this stochasticity on the generation process through bounds on the Kullback-Leibler (KL) divergence, complementing the analysis with numerical and analytical examples. Our main results apply to linear forward SDEs with additive noise and Lipschitz-continuous score functions, and quantify how errors from the prior distribution and score approximation propagate under different choices of the stochasticity parameter. The theoretical bounds are derived using log-Sobolev inequalities for the marginals of the forward process, which enable a more effective control of the KL divergence decay along sampling. For exact score functions, we find that stochasticity acts as an error-correcting mechanism, decreasing KL divergence along the sampling trajectory. For an approximate score function, there is a trade-off between error correction and score error amplification, so that stochasticity can either improve or worsen the performance, depending on the structure of the score error. Numerical experiments on simple datasets and a fully analytical example are included to illustrate and enlighten the theoretical results.

1 Introduction

Score-based diffusion models are a generative modeling framework based on the fact that the process of a stochastic differential equation (SDE) admits a time-reversal process, which is given by another SDE depending on the score of the (forward) distribution [13, 27]. The forward process is used for training, and the reverse process is used for sampling. Since the main interest is in the distribution itself and not in particular paths of the SDE, a whole family of SDEs (i.e. equation (2), with the parameter $\gamma = \gamma(t)$), including an ordinary differential equation (probability flow ODE, corresponding to $\gamma(t) = 0$), can be used for sampling. In this work, we estimate the evolution, along the sampling process, of the Kullback-Leibler divergence (KL divergence), also known as relative entropy, between the generated and the target distributions, as it depends on the free stochasticity parameter of the family of SDEs/ODE, and as it is affected by approximations of the starting sampling distribution (by a known easy-to-sample distribution) and by approximations of the score function (done in the training phase). This partially answers open questions concerning the role of stochasticity in diffusion model sampling [27, 13, 8]. We complement the rigorous theoretical error estimates with numerical experiments on a one-dimensional problem with known exact distribution and score function, a two-dimensional problem, and also with a fully analytical example. In doing so, we shed some light on the influence of these errors and of the different choices of the stochasticity parameter on the quality of the generated distribution.

Diffusion models are currently the state of the art for generative image and video synthesis [22, 4], and are also being used successfully in many scientific and technological applications, such as natural language processing [31], text-to-speech synthesis [30], medical imaging [14], time series analysis [17], protein modeling and design [1, 16], bioinformatics [10], global weather forecasting [21], porous media synthesis [20], and more [29]. Despite their remarkable success in applications, the precise evaluation

of the performance of a generative model presents challenges such as the independent quantification of sample quality and distribution coverage [24, 11]. Sample quality can be informally defined as the plausibility of generated samples in the context of original data, and distribution coverage as the amount to which the original distribution is captured by the generated distribution. Thus, a metric for sample quality should measure how large the density of the generated distribution is in regions where the density of the target distribution is small, and, conversely, a metric for mode coverage should measure how large the target density is where the generated density is small.

The KL divergence of p_1 with respect to p_2 , given by $H(p_1|p_2) := \int p_1 \log(p_1/p_2) dx$, is a standard statistical measure between probability distributions, which, by its asymmetry, provides two possible metrics to compare a generated distribution \tilde{p} with a target distribution p . Both divergences measure sample quality and distribution coverage, but $H(\tilde{p}|p)$ gives more weight to the former, and $H(p|\tilde{p})$ to the latter. This can be seen since the integrand $p(x) \log p(x)/q(x)$ is large when $q(x) \ll p(x)$, and thus regions of X where $q(x) \ll p(x)$ contribute more to the divergence $H(p|q)$ than to $H(q|p)$, and conversely for $p(x) \ll q(x)$. Different applications may be more sensitive either to sample quality or to distribution coverage, making both divergences relevant for evaluating a generative model from a theoretical perspective, even though their use in practice is limited since the densities p, \tilde{p} are usually not available. This work fills a gap in the literature of KL divergence bounds for diffusion models, which typically considers only $H(p|\tilde{p})$ (see Section 1.1). We investigate the impact of stochastic sampling on model performance through both divergences, and, by our use of log-Sobolev inequalities, are able to derive stronger bounds for $H(\tilde{p}|p)$ (associated with sample quality), while the corresponding bound for $H(p|\tilde{p})$ seems more elusive.

For a (forward) SDE

$$dX_t = f(X_t, t) dt + g(t) dW_t, \quad (1)$$

in \mathbb{R}^n , on a time interval $[0, T]$, with probability density $p_t(x)$, where $f = f(x, t)$ and $g = g(t)$ are given and $\{W_t\}_{t \geq 0}$ is an n -dimensional Wiener process, the associated reverse-time SDE takes the form

$$d\tilde{X}_\tau = \left(-\bar{f}(\tilde{X}_\tau, \tau) + \frac{1}{2} \bar{g}^2(\tau) (1 + \gamma(\tau)) \nabla \log \bar{p}_\tau(\tilde{X}_\tau) \right) d\tau + \sqrt{\gamma(\tau)} \bar{g}(\tau) dW_\tau, \quad (2)$$

in the reversed time variable $\tau = T - t$, where $\bar{f}(x, \tau) := f(x, T - \tau)$, $\bar{g}(\tau) := g(T - \tau)$, $\bar{p}_\tau(x) := p_{T - \tau}(x)$, and where $\gamma(\tau) \geq 0$ is arbitrary. It is well known [3, 13] that, under certain conditions, the reverse-time SDE (2) has the same densities of the forward SDE (1) under the change of variables $\tau = T - t$. More precisely, denoting the density associated with (2) by \tilde{p}_τ , if the initial distribution for (2) is $\tilde{p}_0 = \bar{p}_0 = p_T$, then for all $\tau \in (0, T)$ it holds that $\tilde{p}_\tau = \bar{p}_\tau$. A short proof is provided in Section 2.1 for the sake of completeness. Note that (2) gives a family of equations, indexed by the free functional parameter $\gamma(\tau) \geq 0$.

If the (Stein) score function $\nabla \log p(t, \cdot)$ of the forward process given by (1) is known exactly or approximately, for all $0 < t \leq T$, and if at time $t = T$ the distribution p_T is close to a Gaussian distribution or any other distribution which is easy to sample from, the reverse-time SDE (2) can then be used as a generic sampler for p_0 . In practice, the score function $\nabla \log p(t, \cdot)$ can be approximated by a neural network $s_\theta(t, \cdot)$ trained with denoising score-matching [28, 13]. Then, sampling is performed via the approximate reverse-time SDE

$$d\tilde{X}_\tau = \left(-\bar{f}(\tilde{X}_\tau, \tau) + \frac{1}{2} \bar{g}^2(\tau) (1 + \gamma(\tau)) \bar{s}_\theta(\tilde{X}_\tau, \tau) \right) d\tau + \sqrt{\gamma(\tau)} \bar{g}(\tau) dW_\tau, \quad (3)$$

where $\bar{s}_\theta(x, \tau) = s_\theta(x, t - \tau)$ is the reverse-time approximated score. In the machine-learning literature [27], two common choices for γ correspond to setting $\gamma \equiv 0$ (Probability Flow ODE), and $\gamma \equiv 1$ (Anderson/Song's reverse-time SDE).

In summary, the diffusion model algorithm consists of

1. choosing an adequate forward process (1) for which p_T is close to a known and easy-to-sample distribution q ;
2. training a score model $s_\theta(x, t)$ to approximate $\nabla \log p_t(x)$, for all $0 < t \leq T$, by minimizing the global loss function of denoising score-matching;
3. sampling the starting condition \tilde{X}_0 from the prior distribution $q(x) \approx p_T(x)$; and

4. numerically integrating, from $\tau = 0$ to $\tau = T$, the approximate reverse-time equation (3) with the starting condition \tilde{X}_0 .

This pipeline generates a final sample $\tilde{X}_T \sim \tilde{p}_T$, with the aim of \tilde{p}_T being as close as possible to p_0 , the unknown data distribution. Its main sources of error are

- (E1) approximation errors of the score function;
- (E2) approximation errors of the starting prior distribution p_T ;
- (E3) numerical integration errors of the (approximate) reverse-time equation.

This work studies the sampling part of the diffusion algorithm, focusing on the effect of the free parameter γ on the correction and propagation of errors from sources (E1) and (E2). The choice of the integration scheme for solving (3) and the associated numerical errors are also of great importance, but these are not our focus here. Thus, for the theoretical results, we consider the exact solution of either (2) or (3), focusing only on errors (E1) and (E2), while for the numerics we simply use Euler and Euler-Maruyama schemes with a very fine time mesh.

Our work is inspired by a conjecture in Karras et al [13] about the role of stochasticity in equation (2) and by the approach of Markowich and Villani [18] to prove convergence to the stationary distribution for the overdamped Langevin equation. The conjecture is that stochasticity, i.e. a strictly positive $\gamma(t)$, can act as a Langevin-like corrector directing the reverse-time densities \tilde{p}_τ closer to the true forward distributions p_t . Among the many ways to prove convergence towards the stationary distribution of the overdamped Langevin equation, the work in [18] seems to be one of the most natural, using a logarithmic Sobolev inequality (LSI) to obtain a bound which decreases exponentially in the time variable. Our first results (Section 3.1) formalize and prove the conjecture in [13] by adapting the approach in [18] to the reverse-time SDEs with an arbitrary $\gamma(t)$ (equation (2)), while in Section 3.2 we extend these results to the approximate reverse-time SDEs (equation (3)).

In Section 3.1, we consider the SDE (2) with an exact score function and approximate starting prior, addressing the source of error (E2). In this case, the KL divergence in Theorem 1 estimate explicitly demonstrates the advantage of stochasticity, confirming the conjecture in [13]. However, increasing γ makes the problem stiff, adding an effective faster time scale to the dynamics. In practice, this poses a challenge to the numerical approximation of the problem, limiting the choice of γ , as discussed in Section 3.1.1.

Next, in Section 3.2, we consider the more realistic setting of an approximate score function $s(x, t) = \nabla \log p_t(x, t) + \epsilon(x, t)$, where $\epsilon = \epsilon(x, t)$ is the associated error, addressing both errors (E2) and (E1). Here, stochasticity still produces a correction term in the evolution of the generated distribution, but it also amplifies the score error ϵ by a multiplicative factor, making its overall impact more subtle. This behavior reflects empirical findings reported in [8, 13], where the relative performance of stochastic and deterministic sampling varies significantly depending on the dataset and training regime.

In Proposition 3.2, we obtain precise conditions to ensure that the formula for the time derivative of the KL divergence holds. This formula has previously been obtained in the literature by formal arguments, as in [5] for an Ornstein-Uhlenbeck forward process, in the particular case of $\gamma \equiv 1$, and in [2, Lemma 2.22], for a constant γ , in the context of stochastic interpolants. Then, if \tilde{p}_τ satisfies a log-Sobolev inequality with log-Sobolev constant $C(\tau)$, as in (9), Theorem 2 yields the KL divergence estimate

$$H(\tilde{p}_\tau | \tilde{p}_\tau) \leq e^{-\int_0^\tau a(s) ds} H(\tilde{p}_0 | \tilde{p}_0) + \frac{1}{2} \int_0^\tau \bar{g}(s)^2 (1 + \gamma(s)) E_{\tilde{p}_s} [\epsilon_s \cdot \nabla \log h_s] e^{-\int_s^\tau a(r) dr} ds,$$

where $a(s) = C(s)^{-1} \gamma(s) g(s)^2$ and $h_s = \tilde{p}_s / \tilde{p}_s$. When γ is strictly positive, a more explicit estimate is given by equation (25), which eliminates the explicit dependence on $\nabla \log h$ and depends on ϵ only through its $L^2(\tilde{p})$ norm.

In Section 4, we test the theoretical bounds in numerical experiments, comparing with estimated values for the relative entropy. This is done for 1D and 2D Gaussian mixture data distributions, for which accurate entropy estimation is feasible, the score functions are known analytically, and we can also visually compare generated and data distributions. We consider both exact and approximate scores learned by a simple multi-layer-perceptron (MLP), and investigate the effect of score errors on the KL divergence along the sampling path. In particular, we perform a grid search for the best interval to

include stochasticity. Since even for simple datasets reliably estimating $\nabla \log \tilde{p}$ is not straightforward, we conclude by presenting in Section 5 a fully analytical example, based on a single Gaussian dataset, where it is possible to explicitly compare the entropy with the first bound of Theorem 2.

1.1 Related work

There is a large body of recent work that studies convergence bounds for score-based diffusion models. The results obtained by [5] and [7] are the closest to ours, also obtaining bounds in the KL divergence, albeit for $H(p_{\text{data}}|p_{\text{generated}})$ instead of $H(p_{\text{generated}}|p_{\text{data}})$. This difference is due to their use of LSIs for the Gaussian measure, in the forward process, for bounding the prior approximation error, while we use LSIs for the marginals p_t in the sampling process, to account for the entropy decrease induced by the SDE. Therefore, these works focus mainly on bounding errors arising from prior and score approximation and from discretization, without explicitly quantifying the differences between deterministic and stochastic sampling, and without considering a stochasticity parameter other than $\gamma = 1$. There is some overlap in the proof techniques; for example, the formula in our Lemma 2.2 is the formula in Lemma C.1 of [5].

The results in [2, Section 2.4] obtain bounds for $H(p_{\text{data}}|p_{\text{generated}})$, similar to the ones in [5], for more general forward processes in the context of stochastic interpolants. The results consider the general reverse SDE with free stochasticity parameter and establish that the KL divergence of a distribution generated by an SDE is bounded by the score-matching error. In this sense, the score-matching training error effectively controls the KL divergence for SDE sampling, while the same is not ensured for ODE sampling. A similar result was previously obtained by [26] for the reverse SDE with $\gamma = 1$.

Despite the commonalities, our work has the essentially distinct objective of studying the effect of stochasticity in diffusion sampling. Our main contribution consists of using log-Sobolev inequalities for $\nabla \log p_t$ to incorporate an explicit decrease factor in KL divergence along sampling, which can be found in Theorem 2. In the absence of score approximation errors, this results in a decrease in the final entropy; see Theorem 1. We observe that a similar decrease has previously been studied for other metrics, as, for example, in [15]. Moreover, we believe that our numerical experiments, together with the analytical example, can shed light on this phenomenon and orient future research.

Another contribution is to explicitly investigate the conditions required by this kind of bound, without relying on formal arguments. As stated in Corollary 3.1, these are automatically satisfied by time-homogeneous forward processes (such as the EDM, VE and VP processes of [13] and [27]), if the data distribution p_0 has compact support, as in the case of image data. The more general conditions are stated in the Theorems, requiring that the diffused data distributions p_t satisfy a log-Sobolev inequality and the score functions $\nabla \log p_t$ are Lipschitz, which is a hypothesis commonly found in the literature.

2 Background

We mention some background results to be used in the next sections. For completeness, the proofs are provided in Appendix A.1, since these results appear in the literature in a slightly different form.

2.1 SDE facts

Consider a (forward) SDE on the interval $[0, T]$, of the form

$$dX_t = f(X_t, t) dt + g(t) dW_t, \quad (4)$$

where f and g are smooth and such that there exists a unique solution of the corresponding initial-value problem, e.g. with f globally Lipschitz with respect to x , uniformly on $t \in [0, T]$. Let p_t be its associated density, i.e. the solution of the associated Fokker-Planck (FP) equation

$$\frac{\partial p}{\partial t} = -\nabla \cdot (fp) + \frac{1}{2}g^2 \Delta p. \quad (5)$$

As mentioned in Section 1, we extensively use the following result, from [13][Appendix B.5]. Earlier formulations can be found in [3, 27].

Lemma 2.1 (Reverse-time formula). *Consider the family of SDEs given by*

$$d\tilde{X}_\tau = \left(-\bar{f}(\tilde{X}_\tau, \tau) + \frac{1}{2}\bar{g}^2(\tau)(1 + \gamma(\tau))\nabla \log \bar{p}_\tau(\tilde{X}_\tau) \right) d\tau + \sqrt{\gamma(\tau)}\bar{g}(\tau) dW_\tau, \quad (6)$$

for $\tau \in [0, T]$, where $\gamma(\tau)$ is an arbitrary non-negative function, and $\bar{f}(x, \tau) := f(x, T - \tau)$, $\bar{g}(\tau) := g(T - \tau)$ and $\bar{p}_\tau(x) := p_{T-\tau}(x)$. Denote by \tilde{p}_τ^γ its associated probability densities. If the initial densities are the same, i.e. $\tilde{p}_0 = \bar{p}_0$, then the densities \tilde{p}_τ^γ are independent of γ , and we have $\tilde{p}_\tau = p_{T-\tau}$.

Since (6) is an SDE in reverse time that has the same densities of the forward SDE (4), it is called a **reverse-time SDE** associated with (4). Since we formulate this result in a slightly more general form than in [13], we provide a short proof in Appendix A.1.

We will also use the following general lemma, which can be found in [5, Lemma C.1]. Since we are interested in the specific conditions required for this result, we provide a proof in Appendix A.1 showing explicitly where the hypotheses are used.

Lemma 2.2 (Derivative of the KL divergence). *Let p_t and q_t be solutions of the Fokker-Planck equations associated to the SDEs in \mathbb{R}^n*

$$\begin{aligned} dX_t &= a_1(X_t, t) dt + b(t) dW_t^{(1)} \\ dY_t &= a_2(Y_t, t) dt + b(t) dW_t^{(2)}, \end{aligned}$$

where $W^{(1)}, W^{(2)}$ are two independent n -dimensional Wiener processes and a_1, a_2, b are C^1 . If p_t, q_t are bounded above and below by Gaussians, $|\nabla p|, |\nabla q|$ are bounded above by Gaussians, and $a_1, a_2, \nabla \log q_t$ have at most a polynomial growth in x , then the evolution of the KL divergence $H(p_t|q_t)$ is given by

$$\frac{d}{dt} H(p_t|q_t) = -\frac{1}{2}b^2(t) \int \left| \nabla \log \frac{p_t}{q_t} \right|^2 p_t dx + \int (a_1 - a_2) \cdot \left(\nabla \log \frac{p_t}{q_t} \right) p_t dx. \quad (7)$$

2.2 Logarithm-Sobolev Inequalities (LSI)

We recall the definition of the logarithm-Sobolev inequality (LSI), which is known to be important for the exponential convergence towards the asymptotic invariant measure for the Langevin equation and plays a key role in our estimates for the reverse-time SDE, as well.

Definition. *Given a probability density $p(x)$ in \mathbb{R}^n , define the entropy functional as $\text{Ent}_p(f^2) := \int f^2 \log f^2 p dx - \left(\int f^2 p dx \right) \log \left(\int f^2 p dx \right)$. Then, p is said to satisfy a logarithmic Sobolev inequality (LSI) with constant C if*

$$\text{Ent}_p(f^2) \leq 2C \int \|\nabla f\|^2 p dx \quad (8)$$

for any smooth function f .

More explicitly, we use the following consequence of the LSI.

Lemma 2.3. *Condition (8) implies that p satisfies*

$$H(\tilde{p}|p) \leq \frac{C}{2} \int \left| \nabla \log \frac{\tilde{p}}{p} \right|^2 \tilde{p} dx \quad (9)$$

for all probability densities $\tilde{p} \ll p$, i.e. absolutely continuous with respect to p .

3 KL divergence bounds

It is well known that the probability densities $q_t(x)$ associated to the time-independent Langevin equation

$$dX_t = \nabla \log \pi(X_t) dt + \sqrt{2} dW_t \quad (10)$$

converge exponentially to the stationary distribution π when $t \rightarrow \infty$, under some conditions on π [23, 18]. In particular, under the assumption that π satisfies an LSI with constant C , it is obtained, in [18], an exponential bound on the KL divergence, given by

$$H(q_t|\pi) \leq e^{-\frac{2t}{C}} H(q_0|\pi). \quad (11)$$

Thus, deviations in the initial distribution are corrected over time by the Langevin diffusion.

Considering now the reverse-time SDE (6) instead of the Langevin equation, we can aggregate the terms with γ and write it as

$$d\tilde{X}_\tau = \left(-\tilde{f}(\tilde{X}_\tau, \tau) + \frac{1}{2}\tilde{g}^2(\tau)\nabla \log \bar{p}_\tau(\tilde{X}_\tau) \right) d\tau + \left(\frac{1}{2}\tilde{g}^2(\tau)\gamma(\tau)\nabla \log \bar{p}_\tau(\tilde{X}_\tau) d\tau + \sqrt{\gamma(\tau)}\tilde{g}(\tau) dW_\tau \right). \quad (12)$$

Notice that the first term on the right-hand side corresponds to the Probability Flow ODE, i.e. the reverse-time SDE with $\gamma \equiv 0$, and the second is closely related to the Langevin equation (10). Inspired by this form, in [13, Section 4] it is proposed that the reverse-time SDE should be seen as the Probability Flow ODE with the addition of a Langevin-like error-correcting term. This suggests that a bound similar to (11) might be found for the reverse-time SDE.

This idea can be formulated and studied more precisely by considering the KL divergences between the densities \tilde{p}_τ of the reverse-time SDE with some initial density \tilde{p}_0 , and the densities \bar{p}_τ of the reverse-time SDE with initial density $\bar{p}_0 = p_T$, which, by Lemma 2.1, correspond to the densities of the forward SDE. As discussed in Section 1.1, the KL divergence has been a common metric to evaluate the performance of the diffusion algorithm. In Section 3.1, we obtain a result analogous to (11), with \bar{p}_τ assuming the role of the stationary distribution π . Section 3.2 studies the more general case of an approximated reverse-time SDE, in which $\nabla \log \bar{p}_\tau(x)$ is replaced by $s(x, \tau) := \nabla \log \bar{p}_\tau(x) + \epsilon(x, \tau)$, for an approximation error $\epsilon(x, \tau)$.

3.1 Exact score functions

In this section, we consider only the approximation error in the initial condition, that is, when \tilde{p}_τ and \bar{p}_τ are solutions of the same equation (2), but with different initial conditions \tilde{p}_0 and $\bar{p}_0 = p_T$.

Using Lemma 2.2 for \tilde{p}_τ and \bar{p}_τ , with $a_1 = a_2$, we obtain the following result.

Proposition 3.1. *Let \bar{p}_τ and \tilde{p}_τ be as previously defined, and let $\tau \in (0, T)$. If we have that $c_0(t)e^{-c_1(t)|x|^2} < \bar{p}_t(x) < C_0(t)e^{-C_1(t)|x|^2}$ for some time-dependent constants $c_0(t)$, $C_0(t)$, $c_1(t)$, $C_1(t)$, and $\nabla \log \bar{p}_\tau$ is Lipschitz, then the evolution of the KL divergence of \tilde{p}_τ with respect to \bar{p}_τ is given by*

$$\frac{d}{dt}H(\tilde{p}_\tau|\bar{p}_\tau) = -\frac{1}{2}\gamma(\tau)\tilde{g}^2(\tau) \int \left| \nabla \log \frac{\tilde{p}_\tau}{\bar{p}_\tau} \right|^2 \tilde{p}_\tau dx. \quad (13)$$

If, additionally, $\nabla \log \tilde{p}_t$ has at most polynomial growth, we have

$$\frac{d}{dt}H(\tilde{p}_\tau|\bar{p}_\tau) = -\frac{1}{2}\gamma(\tau)\tilde{g}^2(\tau) \int \left| \nabla \log \frac{\tilde{p}_\tau}{\bar{p}_\tau} \right|^2 \bar{p}_\tau dx. \quad (14)$$

Proof. By Lemma 2.2, for equation (13) we only need to show that $|\nabla \tilde{p}_t|$, $|\nabla p_t|$ are sub-Gaussian and \tilde{p}_t has two-sided Gaussian estimates. This follows from Gaussian estimates on the fundamental solution of the Fokker-Planck equation, which we detail in Appendix A.2.

For equation (14), by Lemma 2.2 we need the additional hypothesis that $\nabla \log \tilde{p}_t$ has at most polynomial growth. \square

Proposition 3.1 shows that the KL divergence decreases as τ increases whenever the stochasticity parameter $\gamma(\tau)$ is positive. If $\gamma \equiv 0$, which is the case for the Probability Flow ODE, the entropy remains constant for $\tau \in (0, T)$. However, this result alone is not sufficient to quantify the final entropy decrease due to the dependence of the right hand side of (13) on the unknown \tilde{p}_τ . This can be mitigated by the use of a logarithmic Sobolev inequality.

The forward SDE is typically chosen with a homogeneous linear drift, so that the transition probabilities become Gaussians [27], [13], making the training process viable in practice. We state our main results in the linear case, where the Gaussian estimates for \bar{p}_τ , required by Proposition 3.1, are also satisfied.

Theorem 1. *Let $\bar{p}_\tau, \tilde{p}_\tau$ be as before. If the drift of the forward SDE has the form $f(x, t) = a(t)x$, $p_0 = \bar{p}_T$ is sub-Gaussian, and $\nabla \log \bar{p}_\tau$ is Lipschitz for all $\tau \in (0, T)$, we have the decay estimate on the KL divergence*

$$H(\tilde{p}_\tau | \bar{p}_\tau) \leq e^{-\int_0^\tau C(s)\gamma(s)\bar{g}(s)^2 ds} H(\tilde{p}_0 | \bar{p}_0), \quad (15)$$

for all $\tau \in (0, T)$, where

$$C(\tau) = \begin{cases} C_{LSI}(\tau)^{-1}, & \text{if } \bar{p}_\tau \text{ satisfies an LSI with constant } C_{LSI}(\tau) \\ 0, & \text{otherwise.} \end{cases} \quad (16)$$

If \tilde{p}_T is absolutely continuous with respect to \bar{p}_T , equation (15) also holds for $\tau = T$.

Proof. In the linear case, p_t can be written as the Gaussian convolution $p_t = p_0^t * \mathcal{N}(0, s(t)^2 \sigma(t)^2 I)$, where $p_0^t(x) := p_0(x/s(t))$, see, for example, [13][Appendix B.1]. Then, the hypothesis that \bar{p} has a lower Gaussian bound is satisfied (see Appendix A.2) and thus from Proposition 3.1 we have that, for all $\tau \in (0, T)$,

$$\frac{d}{dt} H(\tilde{p}_\tau | \bar{p}_\tau) = -\frac{1}{2} \gamma(\tau) g(\tau) \int \left| \nabla \log \frac{\tilde{p}_\tau}{\bar{p}_\tau} \right|^2 \tilde{p}_\tau dx \leq 0.$$

If \bar{p}_τ satisfies the log-Sobolev inequality (9) with constant $C_{LSI}(\tau)$, we have

$$\frac{d}{d\tau} H(\tilde{p}_\tau | \bar{p}_\tau) = -\frac{1}{2} \gamma(\tau) g(\tau)^2 \int \left| \nabla \log \frac{\tilde{p}_\tau}{\bar{p}_\tau} \right|^2 \tilde{p}_\tau dx \leq -\frac{1}{C_{LSI}(\tau)} \gamma(\tau) g(\tau)^2 H(\tilde{p}_\tau | \bar{p}_\tau),$$

and thus for all τ we have

$$\frac{d}{d\tau} H(\tilde{p}_\tau | \bar{p}_\tau) \leq -C(\tau) \gamma(\tau) g(\tau)^2 H(\tilde{p}_\tau | \bar{p}_\tau),$$

where $C(\tau) = 1/C_{LSI}(\tau)$ if \bar{p}_τ satisfies an LSI and $C(\tau) = 0$ otherwise. Then, by Grönwall's inequality, we obtain (15). \square

If p_0 is sub-Gaussian, it is known that p_t satisfies an LSI at least for large t [6][Section 4.2]. Moreover, when p_0 has compact support, e.g. for image data, p_t satisfies an LSI for all $t \in (0, T)$ with a dimension-free constant, and $\nabla \log \bar{p}_t$ is automatically Lipschitz. This is summarized by the following corollary.

Corollary 3.1. *If $p_0 = \bar{p}_T$ has compact support with $\text{supp}(p_0) \in B_R(0)$, then $\bar{p}_{T-t} = p_t$ satisfies the hypotheses of Theorem 1 with the dimension-free constant*

$$C_{LSI}(t) = 6s(t)^2(4R^2 + \sigma(t)^2)e^{\frac{4R^2}{\sigma(t)^2}}, \quad (17)$$

where $s(t) := \exp \int_0^t f(s) ds$ and $\sigma(t)^2 := \int_0^t g(s)^2 / s(t)^2 ds$ (in forward time t).

Proof. The constant (17) comes directly from [6, Corollary 1], observing that $p_t = p_0^t * \mathcal{N}(0, s(t)^2 \sigma(t)^2 I)$ with $p_0^t(x) := p_0(x/s(t))$, and that $\text{supp}(p_t^0) \subset B_{s(t)R}(0)$. We then only need to show that $\nabla \log p_t$ is Lipschitz, which is left to Appendix A.2. \square

Remark 3.1. *By the Csiszár-Kullback inequality, which gives $\|p_1 - p_2\|_{\mathcal{L}^1}^2 \leq 2H(p_1 | p_2)$, Theorem 1 gives a corresponding bound on the L^1 distance $\|\tilde{p}_T - p_T\|_{\mathcal{L}^1}$.*

3.1.1 Remark: the functional parameter γ

Since the bound (15) shows a KL divergence decay which is exponential on the stochasticity parameter γ , what is the disadvantage of setting γ arbitrarily large?

The answer is related to the numerical approximation. A simple Euler-Maruyama discretization step of the reverse-time SDE (6) is given by

$$\begin{aligned} X_{\tau_{i+1}} &= X_{\tau_i} + \left(-\bar{f}(X_{\tau_i}, \tau_i) + \frac{1}{2}\bar{g}^2(\tau_i)(1 + \gamma(\tau_i))\nabla \log \bar{p}_{\tau_i}(X_{\tau_i}) \right) \Delta\tau_i + \sqrt{\gamma(\tau_i)\bar{g}(\tau_i)}\sqrt{\Delta\tau_i}\xi \\ &= X_{\tau_i} + \left(-\bar{f}(X_{\tau_i}, \tau_i) + \frac{1}{2}\bar{g}^2(\tau_i)\nabla \log \bar{p}_{\tau_i}(X_{\tau_i}) \right) \Delta\tau_i \\ &\quad + \frac{1}{2}\bar{g}^2(\tau_i)\nabla \log \bar{p}_{\tau_i}(X_{\tau_i})(\gamma(\tau_i)\Delta\tau_i) + \bar{g}(\tau_i)\sqrt{\gamma(\tau_i)\Delta\tau_i}\xi \end{aligned} \quad (18)$$

where $\xi \sim \mathcal{N}(0, 1)$, and $\Delta\tau_i := \tau_{i+1} - \tau_i$. Thus, comparing (18) with (12), one can see that $\gamma(\tau_i)\Delta\tau_i$ gives an effective discretization step size for the Langevin-like part of the reverse-time SDE, which, together with the standard step $\Delta\tau_i$, makes the problem stiff for large γ . Setting γ too large requires a very fine mesh which will inevitably increase the computational cost and potentially produce significant discretization errors. In Section 4, we show the trade-off between error correction and discretization errors in numerical experiments; see Figure 3.

3.2 Approximated score functions

The previous bounds can be readily generalized to the case where the reverse-time SDE depends on an approximated score $s(x, \tau) = \nabla \log \bar{p}_\tau(x) + \epsilon_\tau(x)$, for some error function $\epsilon_\tau(x)$. This models the setting of $s(x, \tau)$ being a neural network trained by score-matching, as in the diffusion model algorithm described in Section 1.

The approximated version of equation (6) is given by

$$d\tilde{X}_\tau = \left(-\bar{f}(\tilde{X}_\tau, \tau) + \frac{1}{2}\bar{g}^2(\tau)(1 + \gamma(\tau)) \left(\nabla \log \bar{p}_\tau(\tilde{X}_\tau) + \epsilon_\tau(\tilde{X}_\tau) \right) \right) d\tau + \sqrt{\gamma(\tau)\bar{g}(\tau)} dW_\tau, \quad (19)$$

with a corresponding Fokker-Planck equation

$$\frac{\partial \tilde{p}}{\partial \tau} = -\nabla \cdot \left(\left(-\bar{f} + \frac{1}{2}\bar{g}^2(\gamma + 1)(\nabla \log \bar{p} + \epsilon) \right) \tilde{p} \right) + \frac{1}{2}\gamma\bar{g}^2\Delta\tilde{p}. \quad (20)$$

Then, we can use Lemma 2.2 to obtain straightforward generalizations of Proposition 3.1 and Theorem 1.

Proposition 3.2. *Let \bar{p}_τ be as before and \tilde{p}_τ be a solution of the perturbed Fokker-Planck (20) with initial condition \tilde{p}_0 . Under the same hypotheses of Proposition 3.1, if $\epsilon(x, \tau)$ is C^1 and such that $\epsilon(\cdot, \tau)$ has at most polynomial growth, we have, for all $\tau \in (0, T)$,*

$$\frac{d}{d\tau} H(\tilde{p}_\tau | \bar{p}_\tau) = \frac{1}{2}\bar{g}^2(1 + \gamma) \int \epsilon \cdot \left(\nabla \log \frac{\tilde{p}_\tau}{\bar{p}_\tau} \right) \tilde{p}_\tau \, dx - \frac{1}{2}\gamma\bar{g}^2 \int \left| \nabla \log \frac{\tilde{p}_\tau}{\bar{p}_\tau} \right|^2 \tilde{p}_\tau \, dx, \quad (21)$$

and, provided that $\nabla \log \tilde{p}_t$ has at most polynomial growth, also that

$$\frac{d}{d\tau} H(\bar{p}_\tau | \tilde{p}_\tau) = \frac{1}{2}\bar{g}^2(1 + \gamma) \int \epsilon \cdot \left(\nabla \log \frac{\tilde{p}_\tau}{\bar{p}_\tau} \right) \bar{p}_\tau \, dx - \frac{1}{2}\gamma\bar{g}^2 \int \left| \nabla \log \frac{\tilde{p}_\tau}{\bar{p}_\tau} \right|^2 \bar{p}_\tau \, dx. \quad (22)$$

Proof. Since the hypotheses of Proposition 3.1 are satisfied, both formulas follow directly from Lemma 2.2 with the assumptions on ϵ_t . \square

Corollary 3.2. *If $\gamma(s) > 0$ for all $s \in (0, \tau)$, then*

$$H(\bar{p}_\tau | \tilde{p}_\tau) \leq H(\bar{p}_0 | \tilde{p}_0) + \frac{1}{8} \int_0^\tau \bar{g}^2 \frac{(1 + \gamma)^2}{\gamma} \left(\int |\epsilon|^2 \bar{p}_s \, dx \right) ds. \quad (23)$$

A corresponding result for the stochastic interpolation framework can be found in [2], Lemma 2.22.

Proof. Using Young's inequality on equation (22), we have that, for every positive function $\eta = \eta(t)$,

$$H(\bar{p}_\tau | \tilde{p}_\tau) \leq H(\bar{p}_0 | \tilde{p}_0) + \frac{1}{2} \int_0^\tau \bar{g}^2 \int \left((1 + \gamma) \eta(s) |\epsilon|^2 + \left(\frac{1 + \gamma}{4\eta(s)} - \gamma \right) \left| \nabla \log \frac{\tilde{p}_s}{\bar{p}_s} \right|^2 \right) \bar{p}_s dx ds.$$

Taking $\eta(s) = (1 + \gamma(s))/4\gamma(s)$, we obtain (23). \square

Corollary 3.2 shows that, for stochastic sampling, it is possible to bound the KL divergence $H(\bar{p}_\tau | \tilde{p}_\tau)$ by a multiple of the score error plus the initial error, as has been observed in the literature ([26], [2]). This is, in fact, a consequence of the entropy decay phenomenon for the SDE, which for the KL divergence $H(\tilde{p} | \bar{p})$ can be better quantified with the use of a log-Sobolev inequality, in the following generalization of Theorem 1.

Theorem 2. *Under the same hypothesis of Theorem 1, if $\epsilon(x, \tau)$ is C^1 and such that $\epsilon(\cdot, \tau)$ has at most polynomial growth, we have that*

$$H(\tilde{p}_\tau | \bar{p}_\tau) \leq e^{-\int_0^\tau \alpha(s) ds} H(\tilde{p}_0 | \bar{p}_0) + \frac{1}{2} \int_0^\tau \bar{g}(s)^2 (1 + \gamma(s)) E_{\tilde{p}_s} \left[\epsilon_s \cdot \nabla \log \frac{\tilde{p}_s}{\bar{p}_s} \right] e^{-\int_s^\tau \alpha(r) dr} ds, \quad (24)$$

with $\alpha(s) := C(s)\gamma(s)g(s)^2$, where $C(s) = 1/C_{LSI}(s)$ if \bar{p}_s satisfies an LSI and $C(s) = 0$ otherwise, as in Theorem 1.

Moreover, if $\gamma(s) > 0$ for all $s \in (0, \tau)$, then, for any $\delta(s)$ satisfying $0 < \delta(s) \leq \gamma(s)$ in $(0, \tau)$, we have

$$H(\tilde{p}_\tau | \bar{p}_\tau) \leq e^{-\int_0^\tau \alpha(s, \delta) ds} H(\tilde{p}_0 | \bar{p}_0) + \frac{1}{8} \int_0^\tau \frac{1}{\delta(s)} \bar{g}(s)^2 (1 + \gamma(s))^2 E_{\tilde{p}_s} [|\epsilon_s|^2] e^{-\int_s^\tau \alpha(r, \delta) dr} ds, \quad (25)$$

where $\alpha(s, \delta) := C(s)\bar{g}(s)^2(\gamma(s) - \delta(s))$.

Proof. 1. As in the proof of Theorem 1, using the log-Sobolev inequality (9) on the derivative of H , given by (21), we obtain

$$\frac{d}{ds} H(\tilde{p}_s | \bar{p}_s) \leq \frac{1}{2} g(s)^2 (1 + \gamma(s)) \int \epsilon_s \cdot (\nabla \log h_s) \tilde{p}_s dx - \frac{1}{C(s)} \gamma(s) g(s)^2 H(\tilde{p}_s | \bar{p}_s),$$

which, by Grönwall's inequality, gives equation (24).

2. For the second claim, we wish to eliminate the unknown term $\nabla \log(\tilde{p}_s/\bar{p}_s)$ from (21). Using Young's inequality, for any $\delta(s) > 0$ we have

$$\int \epsilon_t \cdot \nabla \log h_t \tilde{p}_t dx \leq \int |\epsilon_t| |\nabla \log h_t| \tilde{p}_t dx \leq \int \left(\frac{1}{4\delta_0(t)} |\epsilon_t|^2 + \delta_0(t) |\nabla \log h_t|^2 \right) \tilde{p}_t dx,$$

where $\epsilon(\cdot, t)$ is square-integrable in \tilde{p}_t since it is polynomial and \tilde{p}_t is sub-Gaussian (see a proof of Gaussian estimates in Appendix A.2). Then, if $\delta_0(s) \leq \gamma(s)/(\gamma(s) + 1)$, we have

$$\begin{aligned} \frac{d}{ds} H(\tilde{p}_s | \bar{p}_s) &\leq \frac{1}{8\delta_0} \bar{g}^2 (1 + \gamma) \int |\epsilon|^2 \tilde{p} dx - \frac{1}{2} \bar{g}^2 (\gamma - (\gamma + 1)\delta_0) \int \left| \nabla \log \frac{\tilde{p}}{\bar{p}} \right|^2 \tilde{p} dx \\ &\leq \frac{1}{8\delta_0} \bar{g}^2 (1 + \gamma) \int |\epsilon|^2 \tilde{p} dx - \frac{1}{C_{LSI}} \bar{g}^2 (\gamma - (\gamma + 1)\delta_0) H(\tilde{p} | \bar{p}) \end{aligned} \quad (26)$$

by the LSI. Taking $\delta = (\gamma + 1)\delta_0$ and using Grönwall inequality, we obtain (25). \square

Remark 3.2. 1. In this case, an increase in γ is not clearly related to a decrease in the final entropy.

2. Note that the bound in equation (23) is identical to the one in (25) with $\delta = \gamma$ (that is, ignoring the decay factor), but with the expectation taken in \bar{p}_τ instead of \tilde{p}_τ .

3. Interestingly, in formula (24) the vector $\nabla \log h_s(x) = \nabla \log \tilde{p}_s(x) - \nabla \log \bar{p}_s(x)$ defines a principal direction for the propagation and correction of errors. For example, the component of $\epsilon_s(x)$ perpendicular to $\nabla \log h_s(x)$ does not affect the final entropy $H(\tilde{p}_T|\bar{p}_T)$.
4. Although equation (25) is obtained using an additional inequality, since the inequality is used before the LSI, the bound there can be smaller than the one in equation (24), depending on the tightness of both inequalities. This can be seen in Figure 9, for the analytical example of Section 5.

4 Numerical experiments

In the following experiments, we measure the KL divergence values of distributions evolved through reverse SDEs and ODEs. We show results for the EDM forward process proposed in [13]. We also performed experiments with the Variance Exploding (VE) and Variance Preserving (VP) processes considered in [27], obtaining qualitatively similar results, which can be found in Appendix B.1. The processes are given by the forward SDEs

$$dX_t = \sqrt{2t} dW_t, \quad (\text{EDM})$$

$$dX_t = dW_t, \quad (\text{VE})$$

$$dX_t = -\frac{1}{2}(\beta_1 t + \beta_2)X_t dt + \sqrt{\beta_1 t + \beta_2} dW_t, \quad (\text{VP})$$

which satisfy the linear hypothesis in Theorems 1 and 2.

We consider a simple data distribution p_0 , consisting of the mixture of Gaussians

$$p_0 \sim \theta \mathcal{N}(\mu_1, \sigma_1^2) + (1 - \theta) \mathcal{N}(\mu_2, \sigma_2^2), \quad (27)$$

where $\theta = 0.1$, $\mu_1 = -1$, $\mu_2 = 0.1$, $\sigma_1 = 0.2$, $\sigma_2 = 0.1$. For linear processes, the score functions $\nabla \log p_t$ can be analytically computed, and are Lipschitz (see Appendix A.3), as in the hypotheses of Theorems 1 and 2. We restrict ourselves to a one-dimensional setting for efficient entropy computation and also to allow direct visualization.

The exact prior is given by $p_T = p_0^T * \mathcal{N}(0, s(T)\sigma(T)^2 I)$, as observed in Section 3.1, and following standard practice [13] we use the approximate prior $q_T(x) = \mathcal{N}(0, s(T)\sigma(T)^2 I)$. For the three processes considered, we have that $\lim_{T \rightarrow \infty} H(p_T|q_T) = 0$. Our choice of final forward time T is taken artificially small, so that the initial entropy at $t = T$ is large enough to make the decrease in entropy along sampling perceptible: we use $T = 0.75$ instead of the default choice $T = 80$ [13]. Therefore, our approximate prior should not be seen as a tentative model of standard practice, but as an illustrative example of the phenomenon under study.

The dataset consists of 10^5 samples of the Gaussian mixture distribution (27). The functional parameter $\gamma(t)$ is taken as a constant γ , except at the end of Section 3.2, where it is set to a constant within a given interval $[S_{\min}, S_{\max}]$ and zero outside this interval. Numerical integration is performed with Euler and Euler-Maruyama methods for ODEs and SDEs, respectively, using 500 discretization steps chosen according to the EDM time steps in [13], Table 1. The experiments were performed using the diffusion model package 'diffsci', available at <https://github.com/Lacadame/DiffSci/>.

To avoid confusion, in this section we refer only to the forward time variable t , and consider the densities p_t and \tilde{p}_t in forward time. In this way, diffusion sampling starts at an "initial time" $t = T$ and ends at $t = 0$. We compute relative entropies in two ways. The initial entropy $H(\tilde{p}_T|p_T)$, denoted by H_{init} , is obtained by numerical integration of the densities, which can be calculated analytically for a Gaussian mixture dataset. The final entropies $H(\tilde{p}_0|p_0)$, denoted by H_{ODE} and H_{SDE} , are computed from generated and data samples through the discretization of the empirical densities by an histogram¹. To reduce the dependence on the parameter number of histogram bins, the entropies shown are the mean of the values obtained with bins in the range $\{n_{\text{bins}} - 20, \dots, n_{\text{bins}}\}$. For our dataset, the precision of the entropy estimator was observed to be on the order of 5×10^{-4} .

¹This estimator has limited precision, but it was found to be more reliable than the alternatives, such as using a KDE estimator for the densities or directly using a non-parametric estimator for the entropies.

We calculate the bounds with the log-Sobolev constants obtained in [25]. The χ^2 -divergence for spherical Gaussians $\mu_0 \sim \mathcal{N}(m_0, \sigma_0^2 I)$ and $\mu_1 \sim \mathcal{N}(m_1, \sigma_1^2 I)$ has the closed form

$$\chi^2(\mu_0||\mu_1) = \left(\frac{2\sigma_0^2}{\sigma_1^2(\sigma_0^2 + \sigma_1^2/2)} \right)^{n/2} \exp\left(\frac{\|m_0 - m_1\|^2}{2\sigma_0^2 + \sigma_1^2} \right) - 1. \quad (28)$$

Then, from [25, Corollary 2] we know that the log-Sobolev constant for the Gaussian mixture $\mu_p = p\mu_0 + (1-p)\mu_1$ satisfies

$$C_p \leq \min\{C_0, C_1\}, \quad (29)$$

with

$$\begin{aligned} C_0 &= \max\{\sigma_0^2(1 + (1-p)\lambda_p), \sigma_1^2(1 + p\lambda_p\chi_1)\}, \\ C_1 &= \max\{\sigma_1^2(1 + p\lambda_p), \sigma_0^2(1 + (1-p)\lambda_p\chi_0)\}, \end{aligned}$$

where

$$\lambda_p := \begin{cases} 2 & , p = \frac{1}{2}, \\ \frac{\log p - \log(1-p)}{2p-1} & , p \neq \frac{1}{2}, \end{cases}$$

$$\chi_0 := \chi^2(\mu_0||\mu_1) + 1 \quad \text{and} \quad \chi_1 := \chi^2(\mu_1||\mu_0) + 1.$$

4.1 Exact score functions

First, we generate distributions with exact analytical scores, in the setting of Section 3.1. Figure 1 shows generated distributions and entropy evolution, sampling with exact scores from the approximate prior at initial time T . We can see that the SDE induces a substantial decrease in the relative entropy, higher than that ensured by our bound. The lack of tightness can be attributed to the log-Sobolev constant of p_t , which is valid for *any* q_t but used to a very specific $q_t = \tilde{p}_t$ which is close to p_t .

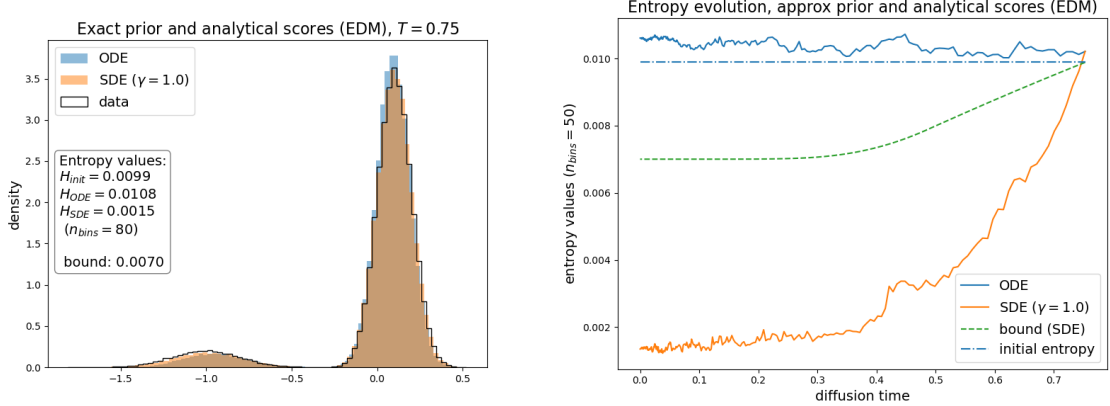


Figure 1: Data and generated distributions with exact score functions (left) and entropy evolution (right).

In Figure 2, we can see the effect of the initial time T on the final entropy, where the discretization grid is fixed and numerical integration initiated from an initial step i such that $t_i \approx T$. Note that SDE sampling produces smaller entropy values for a sufficiently large initial entropy value, associated with a smaller T . This effect is reduced when T is too small, which is expected since then there is not enough time for the stochastic correction to have an effect. The mismatch between initial entropy and final ODE entropy values is due to estimation errors for the latter, since by Proposition 3.1 they should be the same.

Figure 3 shows the effect of γ and the number of discretization steps on the final entropy. Both subfigures show the same data with different horizontal axes: in the left, we can see that there is an optimal interval for γ for each choice of n_{steps} ; and the right column shows that the increase in errors

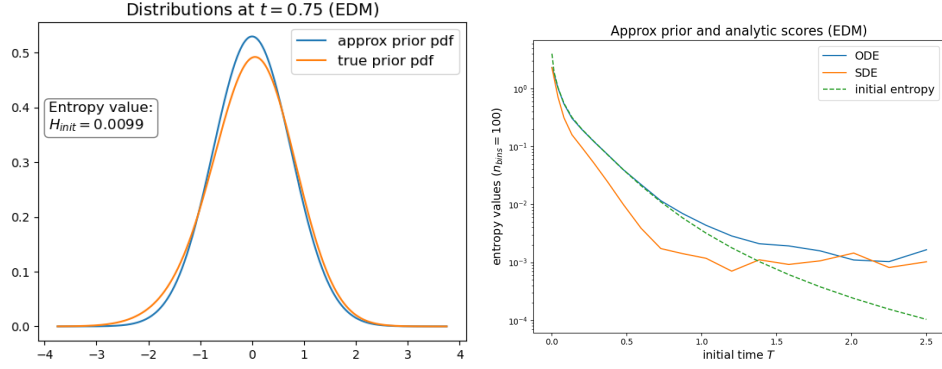


Figure 2: Prior error at a specific T (left) and the effect of initial time T on final entropy values (right).

for large γ is a function of the "effective step size" for the Langevin part of the reverse SDE, given by $\gamma/n_{\text{steps}} \propto \gamma\Delta t$, as discussed in 3.1.1. Equation (18) gives two effective step sizes: $\Delta\tau_i$ for the Flow ODE part, in the first line, and $\gamma(\tau_i)\Delta\tau_i$ for the Langevin-like part in the second line, and for large γ the errors from the second part clearly dominate.

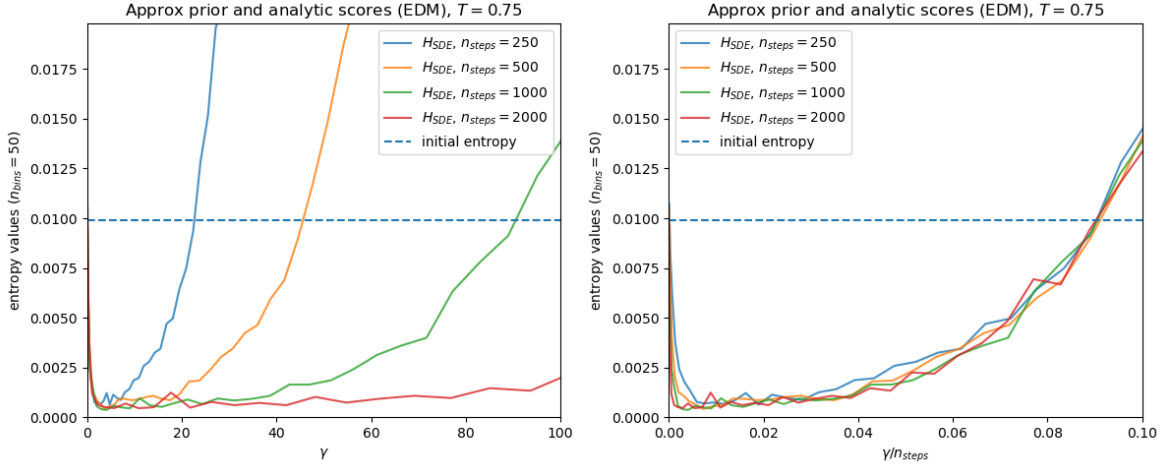


Figure 3: The effect of constant γ and discretization step size on final entropy. The horizontal axis on the right is the 'effective step size' described in 3.1.1.

4.2 Approximated score functions

Here, we sample with learned score functions, in the setting of Section 3.2. The score is approximated by a multi-layer-perceptron (MLP) of size $[100, 100, 100]$ with SiLU activations, trained by denoising score-matching. Figure 4 is an analog of Figure 1 for learned scores, where we also observe a lower entropy value for the SDE. The entropy evolution curves show an initial correction of the prior distribution error by the SDE, followed by the accumulation of score errors near the end of the sampling process. Since $\nabla \log h$ is unknown, we compute only the second bound of Theorem 2, equation (25), using the optimal constant $d := \delta(t)/\gamma(t)$, which in all experiments was found to be $d = 1$. The expectation of the score errors $E_{\tilde{p}}[|\epsilon_t|^2]$ can also be seen in Figure 4.

In addition, Figure 5 shows the results of sampling from exact prior distributions with learned scores. Compared with Figure 4, we can see that the final entropies are similar for the SDE and lower for the ODE. Since in practice the final time T is chosen so that the prior approximation error is small, this setting can be seen as more realistic, and here the difference observed between SDE and ODE becomes very small. We found similar results experimenting with other datasets, often with a greater advantage for the SDE.

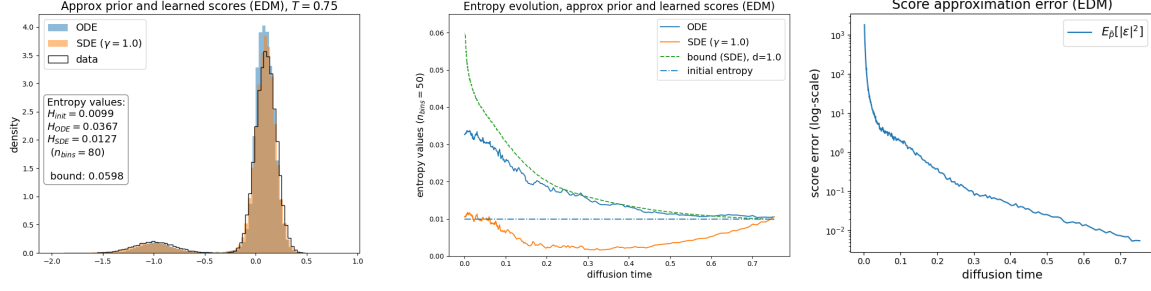


Figure 4: Distributions generated with approximate prior and learned score functions, entropy evolution and $L^2(\tilde{p}_t)$ -norm of the score error.

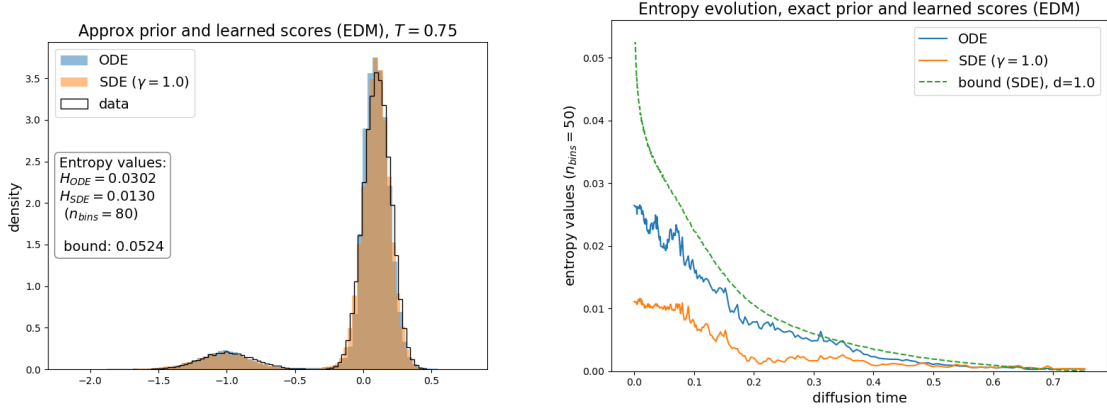


Figure 5: Generated distributions and entropy evolution, with exact prior and learned score functions.

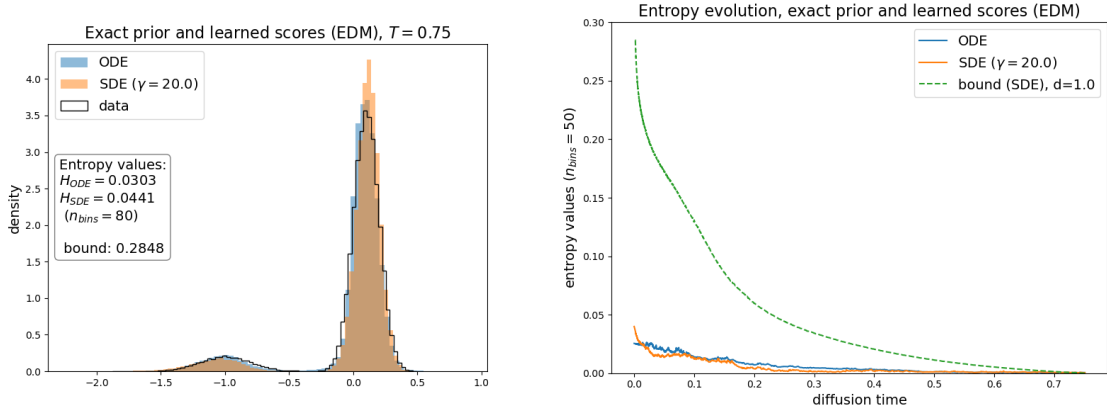
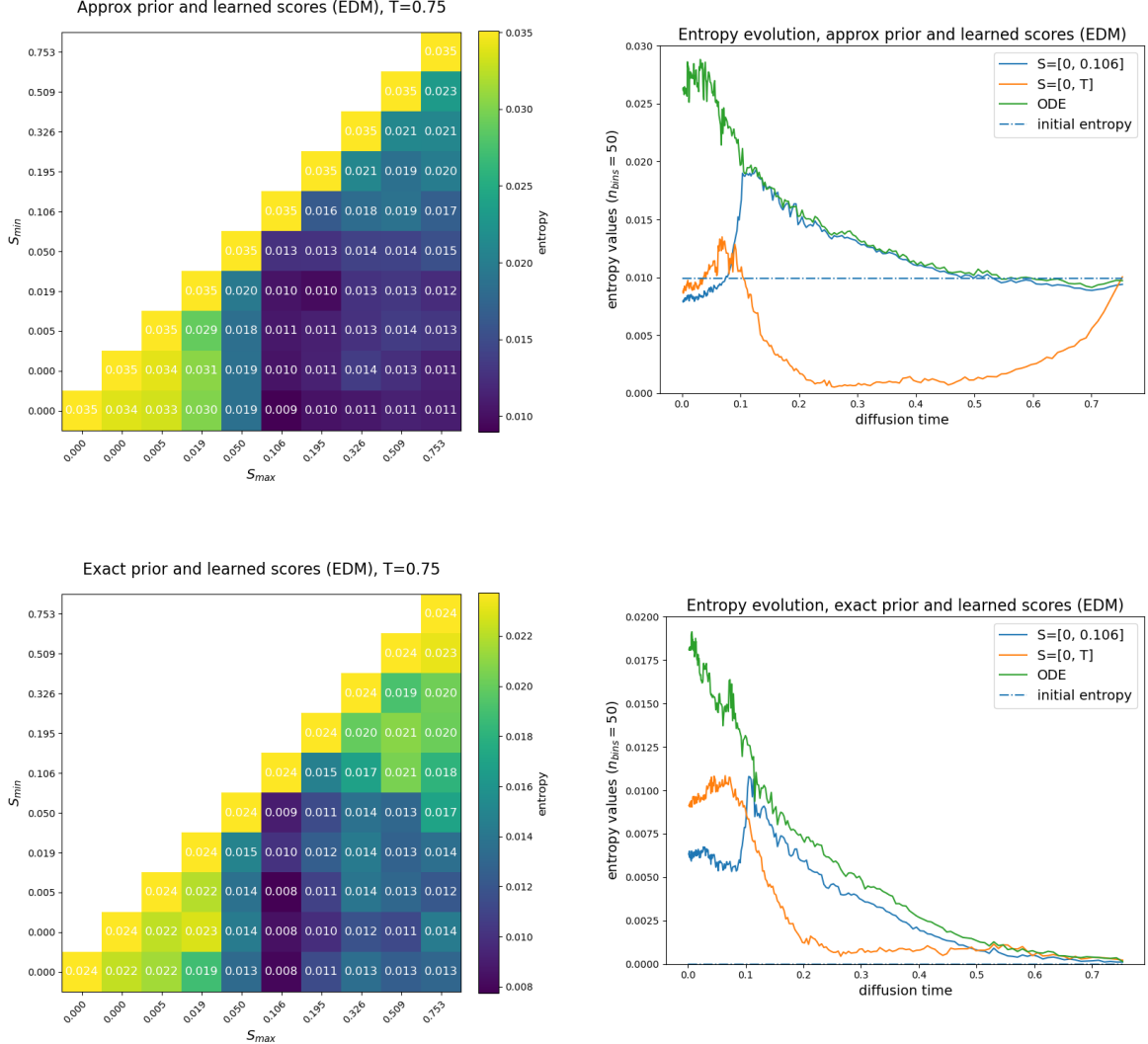


Figure 6: Generated distributions and entropy evolution, with exact prior and learned score functions, for $\gamma = 20$. We also increase the number of steps to 2000, in accordance with the results in Figure 3.

Next, we investigate whether stochasticity has different effects in different time intervals. We set $\gamma(t) = 2$ for $t \in S = [S_{\min}, S_{\max}]$ and $\gamma(t) = 0$ otherwise, and vary the values of S_{\min} and S_{\max} within a fixed grid². Figure 7a shows final entropy values for each interval, where the diagonal entries correspond to the pure ODE and the bottom right entry to the pure SDE. Figure 7b shows the entropy evolution curve of the optimal choice of $[S_{\min}, S_{\max}]$, together with that of the ODE and the SDE. We

²The idea of grid-searching for an optimal zone to introduce stochasticity in diffusion model sampling was previously done by [13] for CIFAR-10 images, using the Fréchet Inception Distance (FID) instead of KL divergence as the relevant metric. However, evolution curves are only possible if the metric can be computed for intermediary distributions, which is not the case for FID.

observe that for both approximate and exact priors, choosing $S_{\max} < T$ leads to the lowest entropy.



(a) Final entropy values, setting $\gamma(t) = 2$ for $t \in [S_{\min}, S_{\max}]$ and $\gamma(t) = 0$ otherwise. (b) Entropy evolution for the optimal choices S_{\min} , S_{\max} from figure (a).

Figure 7: The effect of $\gamma(t)$ on relative entropies, sampling from approximate (top) and exact (bottom) prior with learned scores.

Interestingly, comparing the cases of $S = [0, T]$ with $S = [0, S_{\max}]$, we see that introducing stochasticity before S_{\max} initially reduces the entropy, but induces an increase near the end, in the interval $[0, S_{\min}]$ where both equations are the same. Since in equations (21) and (24) the error contribution factor is given by the expectation of $\langle \nabla \log h_t, \epsilon_t \rangle$, this suggests that early stochasticity changes \tilde{p} in a way that the projection coefficient $\langle \nabla \log h_s, \epsilon_s \rangle$ is increased in average, for $s \approx 0$. This shows that choosing γ so that the entropy increase at each time is minimized does not necessarily imply a lower final entropy, highlighting the value of final bounds such as those in Theorem 2 over the entropy derivative formula in Proposition 3.2.

We also performed this experiment on MLPs with the activation functions ReLU and Softmax, which led to patterns slightly different from those in Figure 7a, as shown in Appendix B.2. We did not find a reliable method for determining the optimal $[S_{\min}, S_{\max}]$ interval, and believe that it is very sensitive to the dataset and the network being used. Interestingly, we find that there are values of $[S_{\min}, S_{\max}]$ which make the final entropy higher than that of the ODE, as can be seen in Figure 15a.

Finally, Figure 8 shows the evolution of the relative entropy $H(p_t|\tilde{p}_t)$, instead of $H(\tilde{p}_t|p_t)$, together with the bound given in Corollary 3.2. Compared with Figure 4, we observe that the SDE produces a slightly larger decrease in this entropy, but the bound here is strictly increasing since it does not account for the decay of entropy. Although we cannot ensure that \tilde{p} satisfies an LSI, the structural similarity between \tilde{p}_t and p_t suggests that this should usually be true.

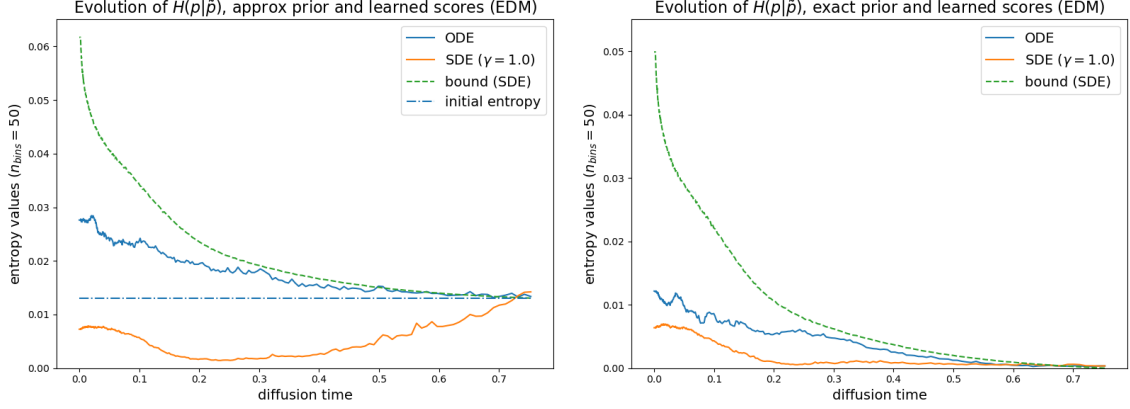


Figure 8: The evolution of the inverse entropy $H(p_t|\tilde{p}_t)$, together with the bound of Corollary 3.2, for the EDM process with learned score functions.

4.3 The effect of non-conservativity

In the ‘Practical considerations’ of [13, Section 4], it is suggested that detrimental effects of stochasticity could be attributed to the non-conservativity of the learned score. The previous experiments, in particular Figures 15a and 6, show that the choice of the interval $S = [S_{\min}, S_{\max}]$ can make stochasticity detrimental even in a 1D setting, where every function is conservative. Moreover, the KL divergence bounds obtained in Section 3.2 do not show an explicit effect of conservativity on error propagation.

To further investigate this point, we perform analogous experiments on a 2D Gaussian mixture dataset to see whether the negative effects of stochasticity are amplified. We found a similar qualitative behavior to the one-dimensional case, even though the learned score functions are not conservative in this case. We refer to Appendix B.3 for more details. Based on this, it seems that conservativity by itself is not a crucial factor in the performance of stochastic sampling, although more nuanced effects could emerge in experiments with high-dimensional real-world data.

5 A fully analytic example

In this section, we consider an example for which we can explicitly compute the KL divergence and the first bound of Theorem 2, allowing a more direct analysis of the effect of the parameter γ . We start by assuming the ‘data’ distribution is a Gaussian $X_0 \sim \mathcal{N}(\mu_0, \sigma_0^2)$ and consider a forward equation of the form

$$dX_t = g(t) dW_t, \quad (30)$$

on a time interval $0 \leq t \leq T$, so the forward process is a Gauss-Markov process $X_t \sim \mathcal{N}(\mu_0, \sigma(t)^2)$, with score function

$$\nabla \log p(x, t) = -\frac{x - \mu_0}{\sigma(t)^2}, \quad \text{where } \sigma(t)^2 = \sigma_0^2 + \int_0^t g(s)^2 ds.$$

We then consider an approximate score of the form

$$s_\theta(x, t) = -\frac{x - \mu_\theta}{\sigma_\theta(t)^2}, \quad \sigma_\theta(t)^2 = \alpha_\theta \sigma(t)^2,$$

with constant parameters $\mu_\theta \in \mathbb{R}$ and $\alpha_\theta > 0$. The error to the exact score, defined in Section 3.2, becomes

$$\epsilon_t(x) = \frac{\mu_\theta(t) - \mu_0}{\sigma_\theta(t)^2} + \left(1 - \frac{\sigma(t)^2}{\sigma_\theta(t)^2}\right) \frac{x - \mu_0}{\sigma(t)^2}. \quad (31)$$

This approximate score yields the family of linear approximate reverse equations

$$d\tilde{X}_\tau = \frac{1}{2}\bar{g}^2(\tau)(1 + \gamma(\tau)) \left(\frac{\tilde{X}_\tau - \bar{\mu}_\theta(\tau)}{\bar{\sigma}_\theta(\tau)^2} \right) d\tau + \sqrt{\gamma(\tau)}\bar{g}(\tau) dW_\tau, \quad (32)$$

in the interval $0 \leq \tau \leq T$. Since this is a linear equation, it can be solved explicitly [12, Section 5.6], yielding the solution

$$\tilde{X}_\tau = e^{-A(\tau)}\tilde{X}_0 + e^{-A(\tau)} \int_0^\tau \bar{\mu}_\theta(s)a(s)e^{A(s)} ds + e^{-A(\tau)} \int_0^\tau \sqrt{\gamma(s)}\bar{g}(s)e^{A(s)} dW_s, \quad (33)$$

where

$$A(\tau) = \int_0^\tau a(s) ds, \quad a(\tau) = \frac{1}{2} \frac{\bar{g}(\tau)^2(1 + \gamma(\tau))}{\bar{\sigma}_\theta(\tau)^2}.$$

Finally, we consider a prior, for the reverse process, which is also Gaussian, $\tilde{X}_0 \sim \mathcal{N}(\mu_T, \sigma_T^2)$. Thus, we obtain

$$\bar{\mu}_\theta(\tau) = e^{-A(\tau)}\mu_T + e^{-A(\tau)} \int_0^\tau \bar{\mu}_\theta(s)a(s)e^{A(s)} ds \quad (34)$$

and

$$\bar{\sigma}_\theta(\tau)^2 = e^{-2A(\tau)}\sigma_T^2 + e^{-2A(\tau)} \int_0^\tau \gamma(s)\bar{g}(s)^2 e^{2A(s)} ds. \quad (35)$$

For more explicit calculations, we further assume

$$\sigma_T^2 = \beta_T \sigma(T)^2, \quad \gamma(t) = \gamma. \quad (36)$$

so the free (constant) parameters for the sampling process are the shape-changing parameters $\alpha_\theta, \beta_T > 0$, the translation parameters $\mu_\theta, \mu_T \in \mathbb{R}$, the stochasticity parameter $\gamma \geq 0$, and the starting time $T > 0$. Besides these, we also have the parameters μ_0, σ_0, σ defining the forward distribution.

Then, the mean-square-error in the score becomes

$$\mathbb{E}_{\tilde{p}_\tau}[\tilde{\epsilon}_\tau^2] = \frac{(\mu_\theta - \mu_0)^2}{\alpha_\theta^2 \bar{\sigma}(\tau)^4} + \left(1 - \frac{1}{\alpha_\theta}\right)^2 \frac{1}{\bar{\sigma}(\tau)^2}. \quad (37)$$

Notice that, since the variance of the forward diffusion increases with time, the error in the score decreases, which coincides with the behavior in the numerical example, where the score is approximated by a neural network trained with denoising score-matching (see e.g. Figure 4).

With the parameters (36), the mean and variance of the Gauss-Markov approximate reverse process become

$$\bar{\mu}_\theta(\tau) = \mu_\theta + \left(\frac{\bar{\sigma}(\tau)^2}{\bar{\sigma}(0)^2} \right)^{\frac{1}{2} \frac{(1+\gamma)}{\alpha_\theta}} (\mu_T - \mu_\theta). \quad (38)$$

and

$$\bar{\sigma}_\theta(\tau)^2 = \begin{cases} \bar{\sigma}(\tau)^2 \left(\frac{\gamma \alpha_\theta}{(1+\gamma) - \alpha_\theta} + \left(\beta_T - \frac{\gamma \alpha_\theta}{(1+\gamma) - \alpha_\theta} \right) \left(\frac{\bar{\sigma}(\tau)^2}{\bar{\sigma}(0)^2} \right)^{\frac{(1+\gamma)}{\alpha_\theta} - 1} \right), & 1 + \gamma \neq \alpha_\theta, \\ \bar{\sigma}(\tau)^2 \left(\beta_T + \gamma \ln \left(\frac{\bar{\sigma}(0)^2}{\bar{\sigma}(\tau)^2} \right) \right), & 1 + \gamma = \alpha_\theta. \end{cases} \quad (39)$$

The KL divergence can be computed as

$$H(\tilde{p}_\tau | \bar{p}_\tau) = \frac{1}{2} \left(\ln \frac{\bar{\sigma}(\tau)^2}{\bar{\sigma}_\theta(\tau)^2} + \frac{\bar{\sigma}_\theta(\tau)^2 + (\mu_0 - \bar{\mu}_\theta(\tau))^2}{\bar{\sigma}(\tau)^2} - 1 \right). \quad (40)$$

In Figure 9, we can see the evolution of entropy and of the two bounds of Theorem 2, for a particular choice of prior and score errors, varying γ . Note that the second bound can, in some cases, be tighter

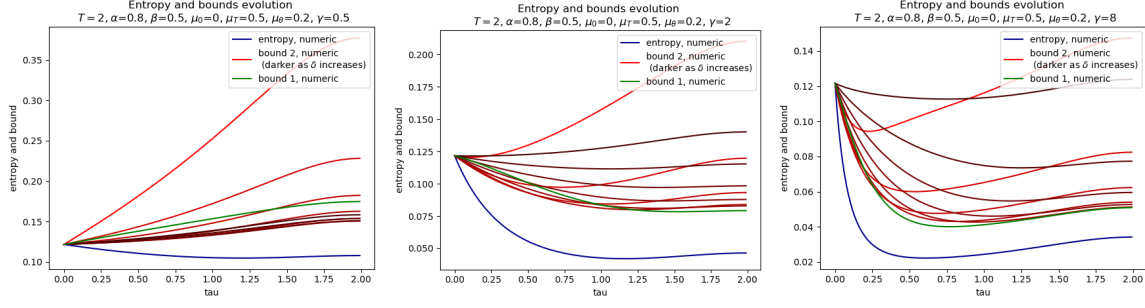


Figure 9: KL divergence and bounds evolution

than the first one, even though its derivation uses one further inequality. This is possible since the extra inequality is applied before the LSI (see the proof of Theorem 2).

Finally, Figure 10 shows the final KL divergence $H(\tilde{p}_0|p_0)$, for many combinations of parameters. Even in this very simple example, we can see that the increase in γ can be beneficial or detrimental, depending on the initial condition and the score error. Interestingly, we can also see that the performance of the SDEs seems to be more stable to variations of the parameters.

Final KL divergence $H(\tilde{p}_0|\bar{p}_0)$ (EDM)

for assorted values of the parameters μ_θ , α_θ , β , and μ_T

■ $\gamma = 0.0$ ■ $\gamma = 1.0$ ■ $\gamma = 5.0$ ■ $\gamma = 20.0$

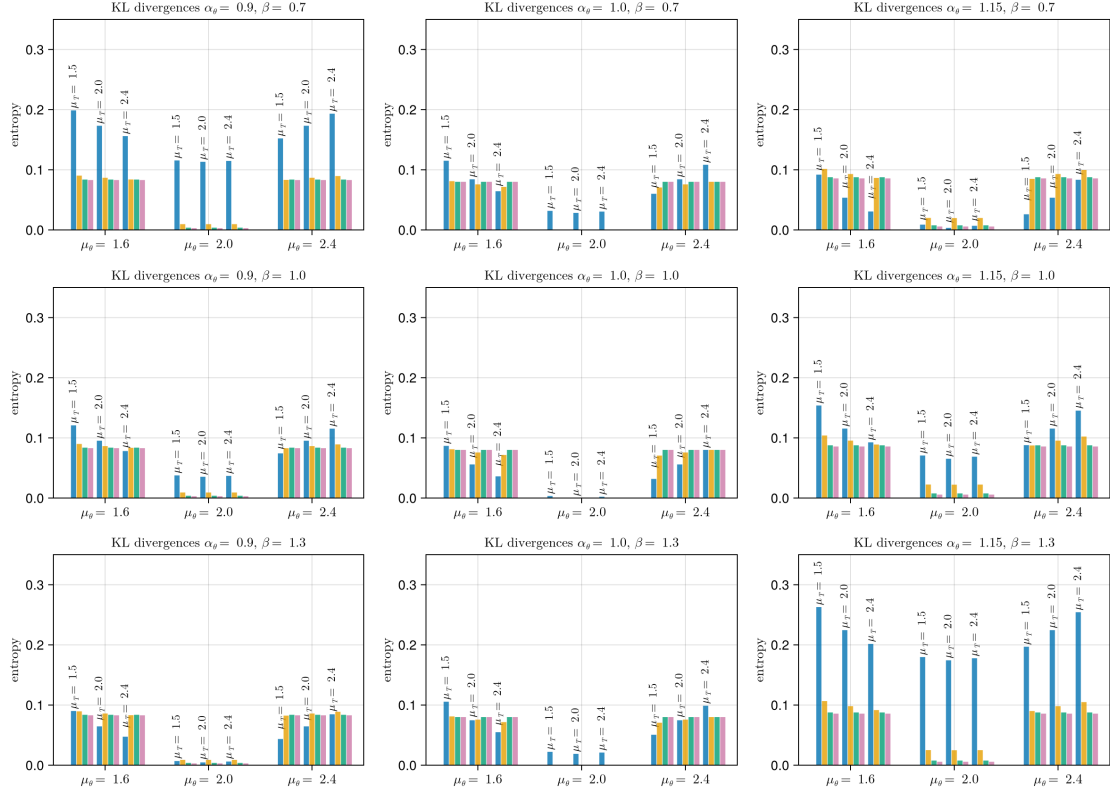


Figure 10: Final KL divergence $H(\tilde{p}_0|p_0)$ for $\gamma = 0.0, 1.0, 5.0, 20.0$, for various choices of the sampling parameters μ_θ , σ_θ , μ_T , and σ_T , with $\mu_0 = 2.0$, $\sigma_0 = 1.0$, $\sigma = 6.0$, and $T = 1.0$.

6 Final Remarks

In this work, we studied the differences between deterministic and stochastic sampling in diffusion models through KL divergence. Theorem 1 showed that, for exact score functions, a positive stochasticity parameter γ implies a reduction in the KL divergence of the generated distribution with respect to the original distribution. This result can be seen as a qualitative explanation of the error-correcting phenomenon observed in stochastic sampling.

When an error is introduced in the score, as in the setting of Theorem 2, the correspondent bound is less informative about the effect of stochasticity, still showing error correction, but also the amplification of new score errors. This is consistent with the findings reported in the literature that stochastic sampling does not always lead to improved results [13], which were observed in our experiments with MLPs on a mixture of Gaussians dataset, and also in a fully analytical case with a single Gaussian dataset. In this respect, the fact that $\nabla \log h_t$ gives a principal direction for error propagation, as observed in Remark 3.2, may be of further interest.

Acknowledgment

The authors acknowledge the support of ExxonMobil Exploração Brasil Ltda. and Agência Nacional de Petróleo, Gás Natural e Biocombustíveis (ANP) through grant no. 23789-1.

References

- [1] J. Abramson, J. Adler, J. Dunger, R. Evans, T. Green, A. Pritzel, O. Ronneberger, L. Willmore, A. Ballard, J. Bambrick, S. Bodenstein, D. Evans, C.-C. Hung, M. O’Neill, D. Reiman, K. Tunyasuvunakool, C. Wu, A. Žemgulytė, E. Arvaniti, and J. Jumper. Accurate structure prediction of biomolecular interactions with alphafold 3. *Nature*, 630:493–500, 05 2024.
- [2] M. S. Albergo, N. M. Boffi, and E. Vanden-Eijnden. Stochastic interpolants: A unifying framework for flows and diffusions, 2023.
- [3] B. D. Anderson. Reverse-time diffusion equation models. *Stochastic Process. Appl.*, 12(3): 313–326, 1982.
- [4] T. Brooks, B. Peebles, C. Holmes, W. DePue, Y. Guo, L. Jing, D. Schnurr, J. Taylor, T. Luhman, E. Luhman, C. Ng, R. Wang, and A. Ramesh. Video generation models as world simulators, 2024. Available at <https://openai.com/research/video-generation-models-as-world-simulators>.
- [5] H. Chen, H. Lee, and J. Lu. Improved analysis of score-based generative modeling: User-friendly bounds under minimal smoothness assumptions. In *International Conference on Machine Learning*, 2022.
- [6] H.-B. Chen, S. Chewi, and J. Niles-Weed. Dimension-free log-sobolev inequalities for mixture distributions. *Journal of Functional Analysis*, 281(11):109236, 2021.
- [7] G. Conforti, A. Durmus, and M. G. Silveri. Kl convergence guarantees for score diffusion models under minimal data assumptions. *SIAM Journal on Mathematics of Data Science*, 7(1):86–109, 2025.
- [8] T. Deveney, J. Stanczuk, L. M. Kreusser, C. Budd, and C.-B. Schönlieb. Closing the ODE-SDE gap in score-based diffusion models through the Fokker-Planck equation [preprint], 2023. Available at <https://arxiv.org/abs/2311.15996>.
- [9] A. Figalli. Existence and uniqueness of martingale solutions for sdes with rough or degenerate coefficients. *Journal of Functional Analysis*, 254(1):109–153, 2008.
- [10] Z. Guo, J. Liu, Y. Wang, M. Chen, D. Wang, D. Xu, and J. Cheng. Diffusion models in bioinformatics and computational biology. *Nature Reviews Bioengineering*, 2(2):136–154, 2024.

- [11] M. Jiralerspong, A. J. Bose, I. Gemp, C. Qin, Y. Bachrach, and G. Gidel. Feature likelihood divergence: evaluating the generalization of generative models using samples. In *Proceedings of the 37th International Conference on Neural Information Processing Systems, NIPS '23*, Red Hook, NY, USA, 2023. Curran Associates Inc.
- [12] I. Karatzas and S. E. Shreve. *Brownian Motion and Stochastic Calculus*. Springer-Verlag New York, 1988.
- [13] T. Karras, M. Aittala, T. Aila, and S. Laine. Elucidating the design space of diffusion-based generative models. *NeurIPS*, 2022. Available at <https://arxiv.org/abs/2206.00364>.
- [14] A. Kazerouni, E. K. Aghdam, M. Heidari, R. Azad, M. Fayyaz, I. Hacihaliloglu, and D. Merhof. Diffusion models for medical image analysis: A comprehensive survey, 2023. Available at <https://arxiv.org/abs/2211.07804>.
- [15] H. Lee, J. Lu, and Y. Tan. Convergence for score-based generative modeling with polynomial complexity, 2023.
- [16] W. Li, X. F. Cadet, D. Medina-Ortiz, M. D. Davari, R. Sowdhamini, C. Damour, Y. Li, A. Miranville, and F. Cadet. From thermodynamics to protein design: Diffusion models for biomolecule generation towards autonomous protein engineering, 2025. Available at <https://arxiv.org/abs/2501.02680>.
- [17] L. Lin, Z. Li, R. Li, X. Li, and J. Gao. Diffusion models for time series applications: A survey, 2023. Available at <https://arxiv.org/abs/2305.00624>.
- [18] P. A. Markowich and C. Villani. On the trend to equilibrium for the Fokker-Planck equation : An interplay between physics and functional analysis. 2004. Available at https://cedricvillani.org/sites/dev/files/old_images/2012/07/P01.MV-FPReview.pdf.
- [19] S. Menozzi, A. Pesce, and X. Zhang. Density and gradient estimates for non degenerate brownian sdes with unbounded measurable drift. *Journal of Differential Equations*, 272:330–369, 2021.
- [20] D. Naiff, B. P. Schaeffer, G. Pires, D. Stojkovic, T. Rapstine, and F. Ramos. Controlled latent diffusion models for 3d porous media reconstruction, 2025. Available at <https://arxiv.org/abs/2503.24083>.
- [21] I. Price, A. Sanchez-Gonzalez, F. Alet, T. R. Andersson, A. El-Kadi, D. Masters, T. Ewalds, J. Stott, S. Mohamed, P. Battaglia, R. Lam, and M. Willson. Gencast: Diffusion-based ensemble forecasting for medium-range weather, 2024. Available at <https://arxiv.org/abs/2312.15796>.
- [22] A. Ramesh, P. Dhariwal, A. Nichol, C. Chu, and M. Chen. Hierarchical text-conditional image generation with clip latents, 2022. Available at <https://arxiv.org/abs/2204.06125>.
- [23] G. O. Roberts and R. L. Tweedie. Exponential convergence of langevin distributions and their discrete approximations. *Bernoulli*, Vol. 2, No. 4. (Dec., 1996), pp. 341-363, 1996.
- [24] M. S. M. Sajjadi, O. Bachem, M. Lucic, O. Bousquet, and S. Gelly. Assessing generative models via precision and recall. In S. Bengio, H. Wallach, H. Larochelle, K. Grauman, N. Cesa-Bianchi, and R. Garnett, editors, *Advances in Neural Information Processing Systems*, volume 31. Curran Associates, Inc., 2018.
- [25] A. Schlichting. Poincaré and log-sobolev inequalities for mixtures. *Entropy*, 21(1), 2019. Available at <https://arxiv.org/pdf/1812.06464>.
- [26] Y. Song, C. Durkan, I. Murray, and S. Ermon. Maximum likelihood training of score-based diffusion models, 2021.
- [27] Y. Song, J. Sohl-Dickstein, D. P. Kingma, A. Kumar, S. Ermon, and B. Poole. Score-based generative modeling through stochastic differential equations. In *International Conference on Learning Representations (ICLR)*, 2021.

- [28] P. Vincent. A connection between score matching and denoising autoencoders. *Neural computation*, 23(7):1661–1674, 2011.
- [29] L. Yang, Z. Zhang, Y. Song, S. Hong, R. Xu, Y. Zhao, W. Zhang, B. Cui, and M.-H. Yang. Diffusion models: A comprehensive survey of methods and applications, 2024. Available at <https://arxiv.org/abs/2209.00796>.
- [30] C. Zhang, C. Zhang, S. Zheng, M. Zhang, M. Qamar, S.-H. Bae, and I. S. Kweon. A survey on audio diffusion models: Text to speech synthesis and enhancement in generative ai, 2023. Available at <https://arxiv.org/abs/2303.13336>.
- [31] H. Zou, Z. M. Kim, and D. Kang. A survey of diffusion models in natural language processing, 2023. Available at <https://arxiv.org/abs/2305.14671>.

A Additional proofs

A.1 Section 2

Here we provide proofs of known results, which are stated in slightly different forms.

of Lemma 2.1. We show that the Fokker-Planck equations associated with both SDEs are the same. Then, the uniqueness hypothesis on (4) ensures that its FP also has a unique solution [9], and thus the associated densities are the same.

To obtain formula (6), consider an arbitrary SDE in reverse time τ , given by $d\hat{X}_\tau = a(\hat{X}_\tau, \tau) d\tau + b(\tau) dW_\tau$. Its FP equation is

$$\frac{\partial p_\tau}{\partial \tau} = -\nabla \cdot (ap_\tau) + \frac{1}{2}b^2\Delta p_\tau,$$

which, changing variables to $t := T - \tau$, becomes

$$\frac{\partial p_t}{\partial t} = \nabla \cdot (\bar{a}p_t) - \frac{1}{2}\bar{b}^2\Delta p_t, \quad (41)$$

with $\bar{a}(x, t) := a(x, T - t)$ and $\bar{b}(t) := b(T - t)$.

To find a and b such that the right-hand sides of (5) and (41) are the same, we can rewrite (5) as

$$\begin{aligned} \frac{\partial p}{\partial t} &= -\nabla \cdot (fp) + \frac{1}{2}g^2\Delta p \\ &= -\nabla \cdot (fp) + \frac{1}{2}g^2((1 + \gamma)\Delta p - \gamma\Delta p) \\ &= -\nabla \cdot (fp) + \frac{1}{2}g^2((1 + \gamma)(\nabla \cdot \nabla p) - \gamma\Delta p) \\ &= -\nabla \cdot (fp) + \frac{1}{2}g^2((1 + \gamma)(\nabla \cdot (p\nabla \log p) - \gamma\Delta p) \quad \text{since } \nabla \log p = \frac{1}{p}\nabla p \\ &= \nabla \cdot \left(\left(-f + \frac{1}{2}g^2(1 + \gamma)\nabla \log p \right) p \right) - \frac{1}{2}g^2\gamma\Delta p, \end{aligned} \quad (42)$$

which is (41) for $\bar{a} = -f + \frac{1}{2}g^2(1 + \gamma)\nabla \log p$ and $\bar{b} = \sqrt{\gamma}g$. This gives exactly equation (6). \square

We observe that, although the statement of Lemma 2.2 can be found in [5, Lemma C.1], its proof there is purely formal. Here, we stated some sufficient regularity/integrability conditions for it, and provide a complete proof.

of Lemma 2.2. Since the coefficients are C^1 , p_t and q_t are also C^1 , and we can differentiate under the integral sign to obtain

$$\begin{aligned} \frac{d}{dt}H(p_t|q_t) &= \int \partial_t \left(p_t(x) \log \frac{p_t(x)}{q_t(x)} \right) dx = \int \partial_t p_t \log \frac{p_t}{q_t} dx + \int \partial_t p_t dx - \int \frac{p_t}{q_x} \partial_t q_t dx \\ &= \int \partial_t p_t \log \frac{p_t}{q_t} dx - \int \frac{p_t}{q_t} \partial_t q_t dx =: I_1 - I_2, \end{aligned}$$

as $\int \partial_t p_t dx = d/dt \int p_t dx = 0$. Substituting the Fokker-Planck equation and integrating by parts, we have

$$I_1 = \int \nabla \cdot \left(a_1 p - \frac{1}{2} b^2 \nabla p \right) \log \frac{p_t}{q_t} dx = \int \left(a_1 p - \frac{1}{2} b^2 \nabla p \right) \cdot \nabla \log \frac{p}{q} dx$$

provided that $a_1 p \log(p/q)$ and $(\nabla p) \log(p/q)$ are both $o(|x|^{n-1})$, and thus the boundary terms vanish at infinity. This follows from the hypotheses, since, by the two-sided Gaussian bounds on p, q , we have

$$\log \frac{p}{q} \leq \log \left(\frac{C_1 e^{-C_2 |x|^2}}{C_3 e^{-C_4 |x|^2}} \right) = C_5 - C_6 x^2, \quad (43)$$

for some constants C_i , and a_1 is also polynomial.

Analogously, we have

$$I_2 = \int \nabla \cdot \left(a_2 q - \frac{1}{2} b^2 \nabla q \right) \frac{p}{q} dx = \int \left(a_2 q - \frac{1}{2} b^2 \nabla q \right) \cdot \nabla \left(\frac{p}{q} \right) dx,$$

as $a_2 p$ and $(\nabla \log q) p$ are both $o(|x|^{n-1})$ by the hypotheses. Using that $\nabla f = f \nabla \log f$, we can write

$$I_1 = \int p \left(a_1 - \frac{1}{2} b^2 \nabla \log p \right) \cdot \nabla \log \frac{p}{q} dx \quad \text{and} \quad I_2 = - \int p \left(a_2 - \frac{1}{2} b^2 \nabla \log q \right) \cdot \nabla \log \frac{p}{q} dx,$$

which gives

$$\begin{aligned} I_1 - I_2 &= \int p \left(a_1 - a_2 - \frac{1}{2} b^2 (\nabla \log p - \nabla \log q) \right) \cdot \nabla \log \frac{p}{q} dx \\ &= -\frac{1}{2} b^2 \int \left| \nabla \log \frac{p}{q} \right|^2 p dx + \int (a_1 - a_2) \cdot \nabla \log \frac{p}{q} p dx. \end{aligned}$$

□

of Lemma 2.3. Since $\tilde{p} \ll p$, we can write $\tilde{p} = f^2 p$. Then, we have

$$\begin{aligned} \text{Ent}_p(f^2) &= \text{Ent}_p \left(\frac{\tilde{p}}{p} \right) = \int \frac{\tilde{p}}{p} \log \frac{\tilde{p}}{p} p dx - \left(\int \frac{\tilde{p}}{p} p dx \right) \log \left(\int \frac{\tilde{p}}{p} p dx \right) \\ &= \int \log \frac{\tilde{p}}{p} \tilde{p} - 1 \log 1 = H(\tilde{p}|p) \end{aligned}$$

and

$$\begin{aligned} \int \left\| \nabla \log \frac{\tilde{p}}{p} \right\|^2 \tilde{p} dx &= \int \left\| \nabla \log f^2 \right\|^2 f^2 p dx = \int \left\| \frac{1}{f^2} 2f \nabla f \right\|^2 f^2 p dx \\ &= 4 \int \left\| \nabla f \right\|^2 p dx. \end{aligned}$$

Therefore, if the LSI holds for p , the second inequality also holds for all such \tilde{p} . □

A.2 Section 3

Here we provide technical details on the proofs of our results in Section 3.

of the Gaussian estimates in the proof of Proposition 3.1. To prove that \tilde{p} has two-sided Gaussian bounds and that $|\nabla \tilde{p}|$ is sub-Gaussian, we use decay estimates for the fundamental solution of the Fokker-Planck equation [19, Theorem 1.2]. In general, if $p_t(x_t|x_0)$ is a fundamental solution of the FP equation of $dX_t = b(X_t, t) dt + \sigma(X_t, t) dW_t$ with σ Hölder and bounded, and b Lipschitz in x , then

$$|p_t(x_t|x_0)| \leq C_1 e^{-c_1 |x_t - \theta_t(x_0)|^2}$$

and

$$|\nabla_{x_t} p_t(x_t|x_0)| \leq C_2 e^{-c_2 |x_t - \theta_t(x_0)|^2},$$

where $C_1, c_1 > 0$ are constant in x , and θ is the deterministic flow associated with the drift, i.e.

$$\frac{d}{dt}\theta_t(x) = b(\theta_t(x), t), \quad \theta_0(x) = x.$$

In the particular case of equation (6), we have $\sigma(x, t) = \sigma(t)$ and the drift $b(x, t) := a(t)\nabla \log p_t(x)$, for some functions σ and a , and $|b(x, t)| \leq c_2(t)x + c_3(t)$ by the Lipschitz hypothesis on $\nabla \log p_t$. Hence, by Grönwall,

$$|\theta(x, t)| \leq |x_0|e^{\int_0^t c_2(s)ds} + e^{\int_0^t c_2(s)ds} \int_0^t c_3(s) ds =: a|x_0| + b.$$

Since $\tilde{p}_0 = \mathcal{N}(0, \sigma(T)I)$, we can write $\tilde{p}_0(x_0) = C_0 e^{-c_0|x_0|^2}$, and thus

$$|\tilde{p}_t(x_t)| = \left| \int \tilde{p}_t(x_t|x_0) \tilde{p}_0(x_0) dx_0 \right| \leq \int C_2 e^{-(c_1|x-\theta_t(x_0)|^2 + c_0|x_0|^2)} dx_0$$

for $C_2 := C_0 C_1$. Note that, for any $0 < \epsilon < 1$,

$$\begin{aligned} c_1|x - \theta_t(x_0)|^2 + c_0|x_0|^2 &\geq \epsilon c_1(|x|^2 - 2\langle x, \theta_t(x_0) \rangle + |\theta_t(x_0)|^2) + c_0|x_0|^2 \\ &\geq \epsilon c_1 \left(|x|^2 - \frac{1}{2}|x|^2 - 2|\theta_t(x_0)|^2 + |\theta_t(x_0)|^2 \right) + c_0|x_0|^2 \\ &= \epsilon c_1 \left(\frac{1}{2}|x|^2 - |\theta_t(x_0)|^2 \right) + c_0|x_0|^2 \\ &\geq \epsilon c_1 \left(\frac{1}{2}|x|^2 - (a|x_0| + b)^2 \right) + c_0|x_0|^2 \\ &\geq \epsilon c_1 \left(\frac{1}{2}|x|^2 - 2a^2|x_0|^2 - 2b^2 \right) + c_0|x_0|^2 \\ &= \epsilon \frac{c_1}{2}|x|^2 + (c_0 - 2\epsilon c_1 a^2)|x_0|^2 - 2\epsilon c_1 b^2 =: c_2|x|^2 + c_3|x_0|^2 + c_4. \end{aligned}$$

Taking $\epsilon < \min \left\{ 1, \frac{c_0}{2c_1 a^2} \right\}$, we have $c_3 > 0$, and thus

$$\begin{aligned} |\tilde{p}_t(x_t)| &\leq \int C_2 e^{-(c_1|x-\theta_t(x_0)|^2 + c_0|x_0|^2)} dx_0 \leq \int C_2 e^{-(c_2|x|^2 + c_3|x_0|^2 + c_4)} dx_0 \\ &= C_2 e^{-(c_2|x|^2 + c_4)} \int e^{-c_3|x_0|^2} dx_0 = C e^{-c|x|^2} \end{aligned}$$

for some constants $C, c > 0$. An exactly analogous argument shows the decay for $\nabla \tilde{p}_t$. \square

of the lower Gaussian bound in Theorem 1. Since p_t can be written as the Gaussian convolution $p_t = p_0^t * \mathcal{N}(0, s(t)^2 \sigma(t)^2 I)$, with $p_0^t(x) := p_0(x/s(t))$, we have

$$\begin{aligned} p_t(x) &= C(t) \int p_0^t(y) e^{-c(t)|x-y|^2} dy \\ &\geq C(t) \int p_0^t(y) e^{-c(t)(|x|^2 + |y|^2)} dy \\ &= C(t) e^{-c(t)|x|^2} \int p_0^t(y) e^{-c(t)|y|^2} dy = C_2(t) e^{-c(t)|x|^2} \end{aligned}$$

for $c(t), C(t)$ constants in x and $C_2(t) = \int p_0^t(y) e^{-c(t)|y|^2} dy < \infty$ since $p_0^t(x)$ a probability density and $e^{-c(t)|y|^2}$ is bounded. \square

of Corollary 3.1. To show that $\nabla \log p_t$ is Lipschitz in this case, denote the Gaussian pdf by

$$g_t(x) := \frac{1}{(2\pi t^2)^{\frac{1}{n}}} e^{-\frac{|x|^2}{2t^2}},$$

where $x \in \mathbb{R}^n$, and note that

$$\nabla \log p_t(x) = \frac{\nabla(p_0 * g_t)(x)}{p_t(x)} = \frac{p_0 * \nabla g_t(x)}{p_t(x)} = \frac{\int p_0(y) \frac{y-x}{t^2} g_t(x-y) dy}{p_t(x)} = \frac{1}{t^2} \left(-x + \frac{m_t(x)}{p_t(x)} \right),$$

where $m_t(x) := \int p_0(y) y g_t(x-y) dy$.

To see that $m_t(x)/p_t(x)$ is Lipschitz, note that $\nabla(m_t(x)/p_t(x))$ is bounded, since

$$\begin{aligned}
\nabla \left(\frac{m_t(x)}{p_t(x)} \right) &= \frac{\nabla m_t(x)}{p_t(x)} - m_t(x) \frac{\nabla p_t(x)}{p_t(x)^2} \\
&= \frac{\frac{1}{t^2} \int p_0(y) y (y-x) g_t(x-y) dy}{p_t(x)} - m_t(x) \frac{\frac{1}{t^2} \int p_0(y) (y-x) g_t(x-y) dy}{p_t(x)^2} \\
&= \frac{1}{t^2} \left(\frac{\int p_0(y) y^2 g_t(x-y) dy}{p_t(x)} - \frac{x m_t(x)}{p_t(x)} - \frac{m_t(x)^2}{p_t(x)^2} + m_t(x) \frac{x}{p_t(x)} \right) \\
&= \frac{1}{t^2} \left(\frac{\int p_0(y) y^2 g_t(x-y) dy}{p_t(x)} - \frac{m_t(x)^2}{p_t(x)^2} \right) \\
&\leq \frac{1}{t^2} \left(\frac{\int p_0(y) R^2 g_t(x-y) dy}{p_t(x)} + \left(\frac{\int p_0(y) R g_t(x-y) dy}{p_t(x)} \right)^2 \right) = \frac{2R^2}{t^2},
\end{aligned}$$

using that $\text{supp } p_0 \subset B_R(0)$. □

A.3 Section 4

As discussed in the last section (proof of Theorem 1), p_t can be written as the Gaussian convolution $p_t = p_0^t * \mathcal{N}(0, s(t)^2 \sigma(t)^2 I)$, where $p_0^t(x) := p_0(x/s(t))$. If p_0 is the mixture of Gaussians $p_0 = \sum_{l=1}^n w_l \mathcal{N}(\mu_l, \sigma_l^2 I)$, we have $p_0^t = \sum_{l=1}^n w_l \mathcal{N}(s(t)\mu_l, s(t)^2 \sigma_l^2 I)$ and thus

$$\begin{aligned}
p_t &= p_0^t * \mathcal{N}(0, s(t)^2 \sigma(t)^2 I) \\
&= \sum_{l=1}^n w_l \mathcal{N}(s(t)\mu_l, s(t)^2 \sigma_l^2 I) * \mathcal{N}(0, s(t)^2 \sigma(t)^2 I) \\
&= \sum_{l=1}^n w_l \mathcal{N}(s(t)\mu_l, s(t)^2 (\sigma_l^2 + \sigma(t)^2) I),
\end{aligned}$$

is also a mixture of spherical Gaussians. Therefore, the following lemma ensures that $\nabla \log p_t$ is Lipschitz for all $t \in [0, T]$.

Lemma A.1. *The score function of a mixture of finitely many spherical Gaussians is globally Lipschitz.*

Proof. Let p be a mixture of n spherical Gaussians in \mathbb{R}^d given by

$$p(x) = \sum_{l=1}^n w_l \mathcal{N}(x; \mu_l, \sigma_l^2 I), \quad (44)$$

where $\mathcal{N}(x; \mu, \sigma^2 I)$ is the Gaussian pdf with mean μ and covariance matrix $\sigma^2 I$, and $\sum w_l = 1$ with $w_l > 0$. Then the score function is given by

$$\nabla \log p(x) = \frac{\nabla p(x)}{p(x)} = \frac{\sum_{l=1}^n w_l \left(\frac{\mu_l - x}{\sigma_l^2} \right) \mathcal{N}(x; \mu_l, \sigma_l^2 I)}{\sum_{l=1}^n w_l \mathcal{N}(x; \mu_l, \sigma_l^2 I)}, \quad (45)$$

and, writing $\mathcal{N}_l := \mathcal{N}(x; \mu_l, \sigma_l^2 I)$, we have

$$\begin{aligned}
\partial_{x_i x_j}^2 (\log p(x)) &= \partial_{x_j} \left(\frac{\partial_{x_i} p(x)}{p(x)} \right) = \frac{p(x) \partial_{x_i x_j}^2 p(x) - \partial_{x_i} p(x) \partial_{x_j} p(x)}{p(x)^2} \\
&= \frac{\left(\sum_{l=1}^n w_l \left(\frac{(\mu_l^{(i)} - x_i)(\mu_l^{(j)} - x_j)}{\sigma_l^4} - \frac{\delta_{ij}}{\sigma_l^2} \right) \mathcal{N}_l \right) \sum_{l=1}^n w_l \mathcal{N}_l}{\left(\sum_{l=1}^n w_l \mathcal{N}_l \right)^2} \\
&\quad - \frac{\left(\sum_{l=1}^n w_l \left(\frac{\mu_l^{(i)} - x_i}{\sigma_l^2} \right) \mathcal{N}_l \right) \left(\sum_{l=1}^n w_l \left(\frac{\mu_l^{(j)} - x_j}{\sigma_l^2} \right) \mathcal{N}_l \right)}{\left(\sum_{l=1}^n w_l \mathcal{N}_l \right)^2} \\
&= \frac{\sum_{l,k} w_l w_k \mathcal{N}_l \mathcal{N}_k \left(\frac{(\mu_l^{(i)} - x_i)(\mu_k^{(j)} - x_j)}{\sigma_l^4} - \frac{\delta_{ij}}{\sigma_l^2} \right)}{\sum_{l,k} w_l w_k \mathcal{N}_l \mathcal{N}_k} \\
&\quad - \frac{\sum_{l,k} w_l w_k \mathcal{N}_l \mathcal{N}_k \left(\frac{(\mu_l^{(i)} - x_i)(\mu_k^{(j)} - x_j)}{\sigma_l^2 \sigma_k^2} \right)}{\sum_{l,k} w_l w_k \mathcal{N}_l \mathcal{N}_k}.
\end{aligned}$$

Thus

$$\begin{aligned}
\partial_{x_i x_j}^2 (\log p(x)) &= \sum_{l,k} \frac{w_l w_k \mathcal{N}_l \mathcal{N}_k}{\sum_{l',k'} w_{l'} w_{k'} \mathcal{N}_{l'} \mathcal{N}_{k'}} \left(\frac{(\mu_l^{(i)} - x_i)(\mu_l^{(j)} - x_j)}{\sigma_l^4} - \frac{(\mu_l^{(i)} - x_i)(\mu_k^{(j)} - x_j)}{\sigma_l^2 \sigma_k^2} - \frac{\delta_{ij}}{\sigma_l^2} \right) \\
&=: \sum_{l,k} A_{lk}(x)
\end{aligned}$$

To show that this function is bounded, consider the indices l_m such that $\sigma_{l_m} = \sigma_*$ is the largest variance. For all m , we have

$$|A_{l,k}| \leq \frac{w_l w_k \mathcal{N}_l \mathcal{N}_k}{w_{l_m}^2 \mathcal{N}_{l_m}^2} \left| \frac{(\mu_l^{(i)} - x_i)(\mu_l^{(j)} - x_j)}{\sigma_l^4} - \frac{(\mu_l^{(i)} - x_i)(\mu_k^{(j)} - x_j)}{\sigma_l^2 \sigma_k^2} - \frac{\delta_{ij}}{\sigma_l^2} \right|, \quad (46)$$

which vanishes with $|x| \rightarrow \infty$ for all pair (l, k) not satisfying $\sigma_l = \sigma_k = \sigma_*$.

If $\sigma_l = \sigma_k = \sigma_*$, we consider two cases. If $l = k$, we have that

$$\begin{aligned}
|A_{ll}| &= \frac{w_l^2 \mathcal{N}_l^2}{\sum_{l,k} w_l w_k \mathcal{N}_l \mathcal{N}_k} \left| \frac{(\mu_l^{(i)} - x_i)(\mu_l^{(j)} - x_j)}{\sigma_*^4} - \frac{(\mu_l^{(i)} - x_i)(\mu_l^{(j)} - x_j)}{\sigma_*^4} - \frac{1}{\sigma_*^2} \right| \\
&= \frac{w_l^2 \mathcal{N}_l^2}{\sum_{l,k} w_l w_k \mathcal{N}_l \mathcal{N}_k} \left(\frac{1}{\sigma_*^2} \right) \leq \frac{1}{\sigma_*^2}.
\end{aligned}$$

If $l \neq k$, denoting $a = (\mu_l^{(i)} - x_i)$, $b = (\mu_l^{(j)} - x_j)$, $c = (\mu_k^{(i)} - x_i)$ and $d = (\mu_k^{(j)} - x_j)$, we have that

$$A_{lk} + A_{kl} = \frac{w_l w_k \mathcal{N}_l \mathcal{N}_k}{\sum_{l',k'} w_{l'} w_{k'} \mathcal{N}_{l'} \mathcal{N}_{k'}} \left(\frac{ab - ad + cd - cb}{\sigma_*^4} - \frac{2\delta_{ij}}{\sigma_*^2} \right).$$

Using that $ab - ad + cd - cb = (a - c)(b - d)$, we have

$$\begin{aligned}
|A_{lk} + A_{kl}| &= \frac{w_l w_k \mathcal{N}_l \mathcal{N}_k}{\sum_{l',k'} w_{l'} w_{k'} \mathcal{N}_{l'} \mathcal{N}_{k'}} \left| \frac{(\mu_l^{(i)} - \mu_k^{(i)})(\mu_l^{(j)} - \mu_k^{(j)})}{\sigma_*^4} - \frac{2\delta_{ij}}{\sigma_*^2} \right| \\
&\leq \left| \frac{(\mu_l^{(i)} - \mu_k^{(i)})(\mu_l^{(j)} - \mu_k^{(j)})}{\sigma_*^4} - \frac{2\delta_{ij}}{\sigma_*^2} \right|,
\end{aligned}$$

which is constant in x . Therefore

$$\left| \partial_{x_i x_j}^2 (\log p(x)) \right| = \left| \sum_{l,k} A_{lk}(x) \right| \leq \sum_{l=k} |A_{lk}(x)| + \sum_{l < k} |A_{lk}(x) + A_{kl}(x)|$$

is bounded for all i, j , and thus $\nabla \log p(x)$ is Lipschitz. \square

B Additional experiments

B.1 Other forward processes

Here, we present results from numerical experiments analogous to those presented in Section 4, for the three processes, in Figures 11, 12, 13 and 14. The final times T are chosen so that the processes have approximately the same initial entropy, as can be seen in Figure 11.

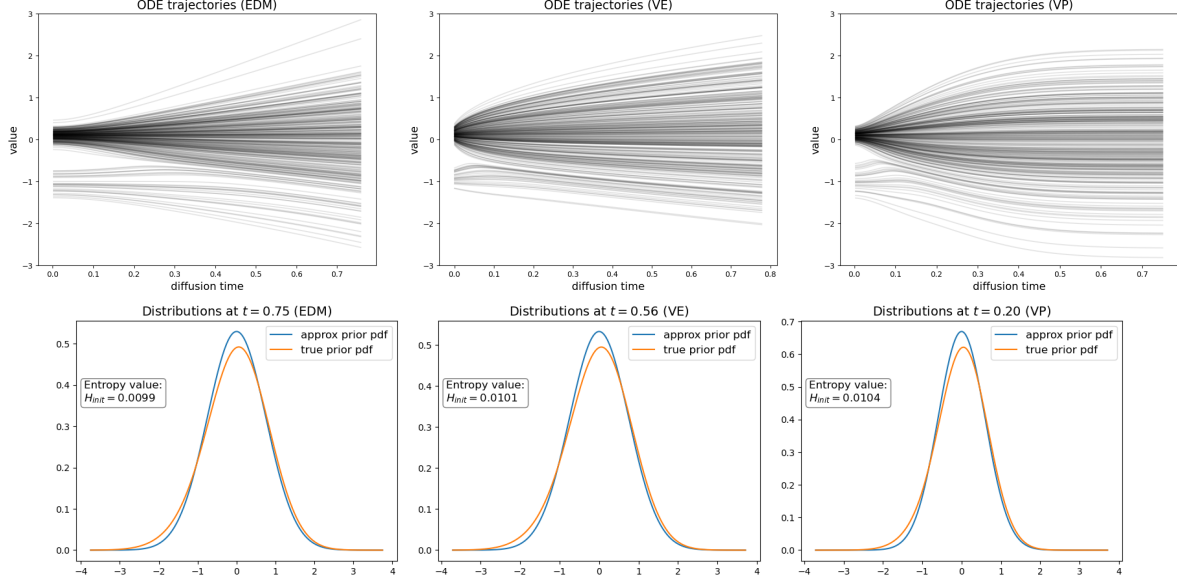


Figure 11: ODE trajectories with exact scores (top) and approximate initial densities (bottom), for the three processes.

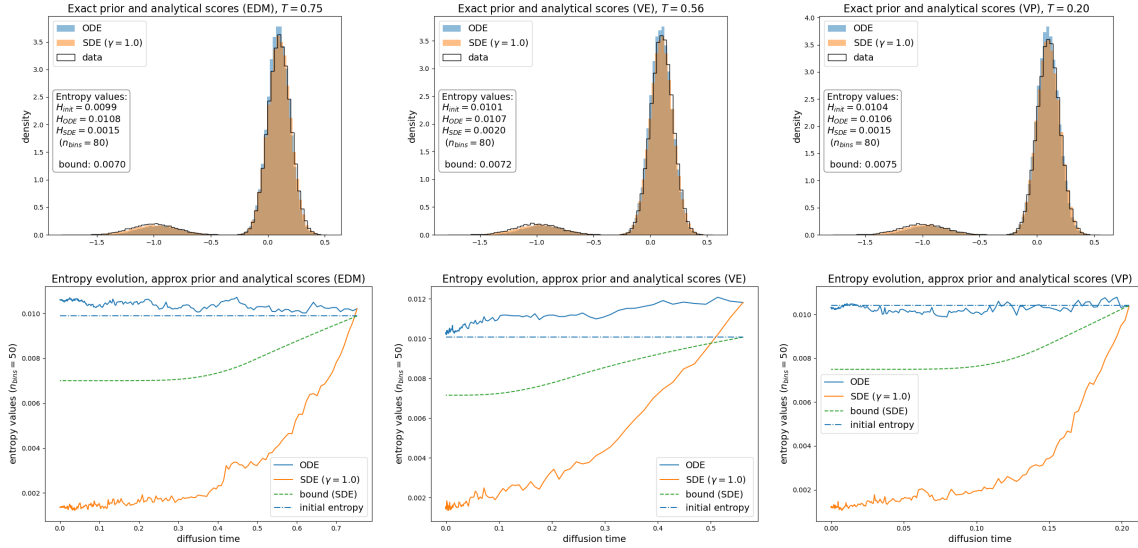


Figure 12: Data and generated distributions for the three processes, with exact score functions, together with entropy evolution. Note that the horizontal axes have different time scales.

B.2 Other activation functions

In Figure 15, we show the final entropy for different intervals $[S_{min}, S_{max}]$, on MLPs with Softplus and ReLU activations. Interestingly, we can see that the optimal choice for the ReLU network has

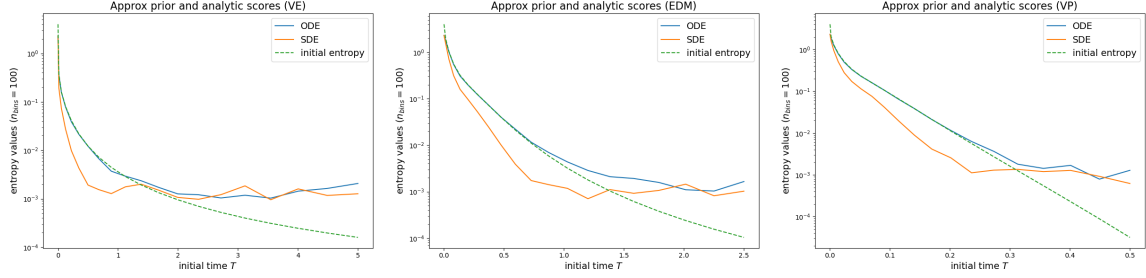


Figure 13: The effect of initial time T on final entropy values.

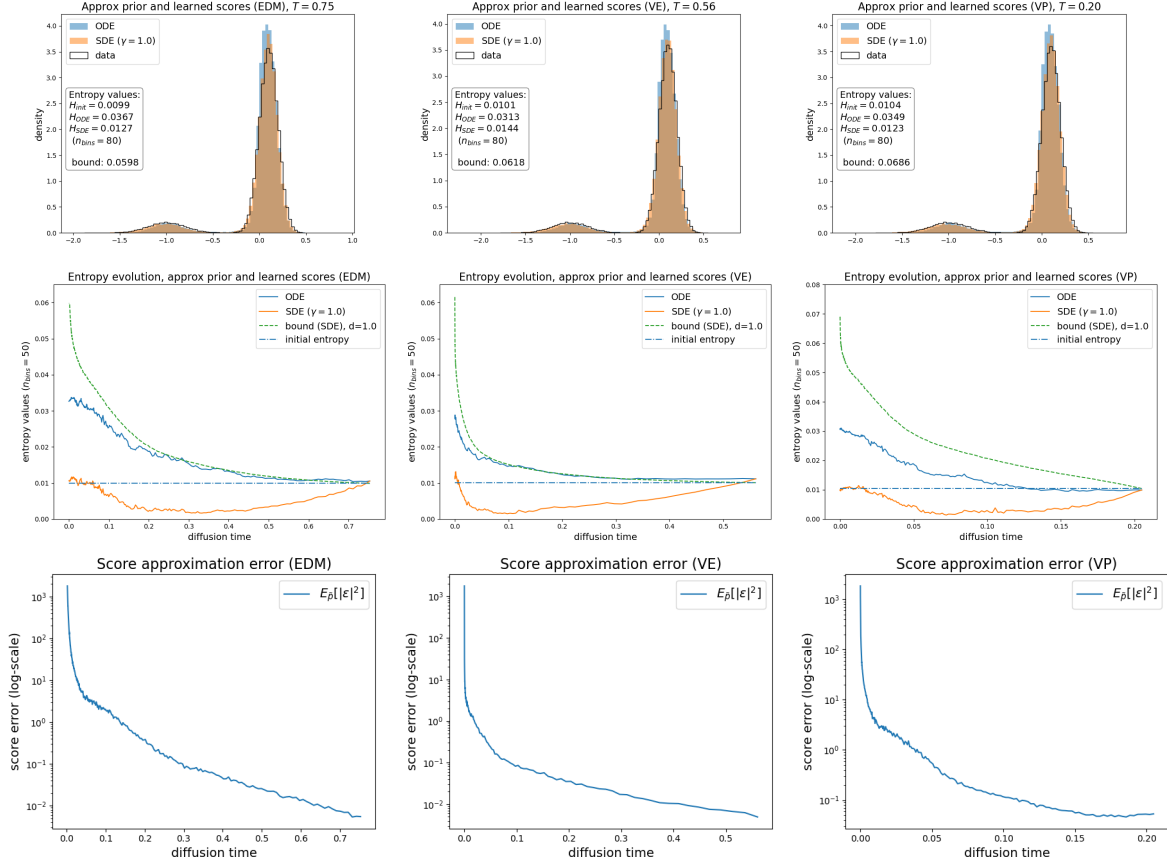
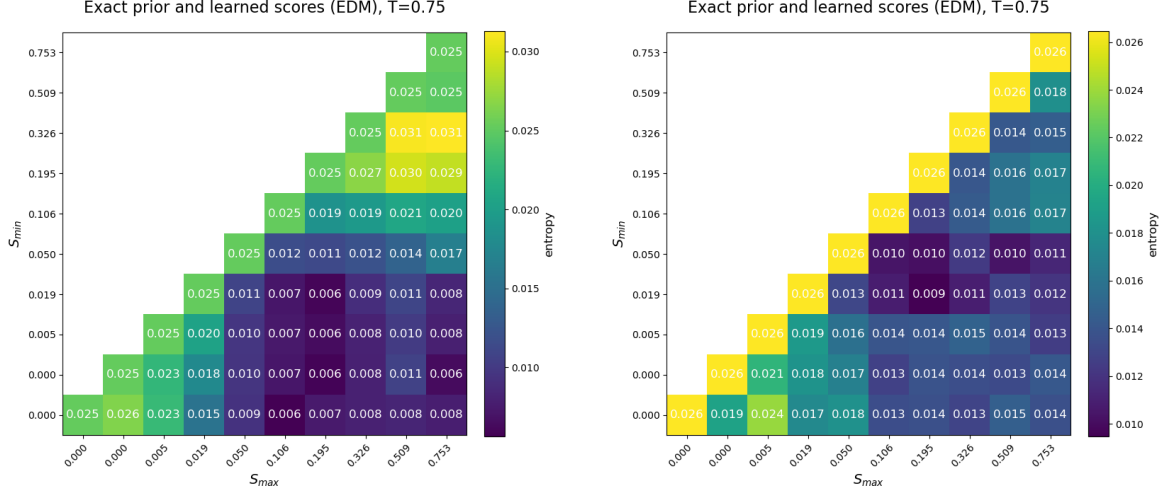


Figure 14: Generated distributions (top), entropy evolution (middle) and $L^2(\tilde{p}_t)$ -norm of the score error (bottom) for the three processes, with approximate prior and learned score functions. Note that the horizontal axes have different time scales.

$S_{\min} > 0$. Moreover, some choices of $[S_{\min}, S_{\max}]$ for the Softplus network make the SDE worse than the ODE.

B.3 2D dataset

We performed analogous experiments on the 2D Gaussian mixture dataset, shown in the top left of Figure 16, to see whether the negative effects of stochasticity are amplified. In Figure 16 we can see a qualitative behavior similar to that of the one-dimensional case, even though the learned score functions are not conservative, as shown on the bottom right by the relative antisymmetry of the



(a) MLP with Softplus activation functions.

(b) MLP with ReLU activation functions.

Figure 15: The effect of $[S_{\min}, S_{\max}]$ on relative entropies, for MLPs with different activation functions.

Jacobian $J = \nabla_x s_\theta(\cdot, t)$, given by

$$A(x, t) := \frac{\|J(x, t) - J^T(x, t)\|_F}{\|J(x, t)\|_F}, \quad (47)$$

averaged from 1000 samples of $x \sim p_t$ for each t , where $\|\cdot\|_F$ is the Frobenius norm.

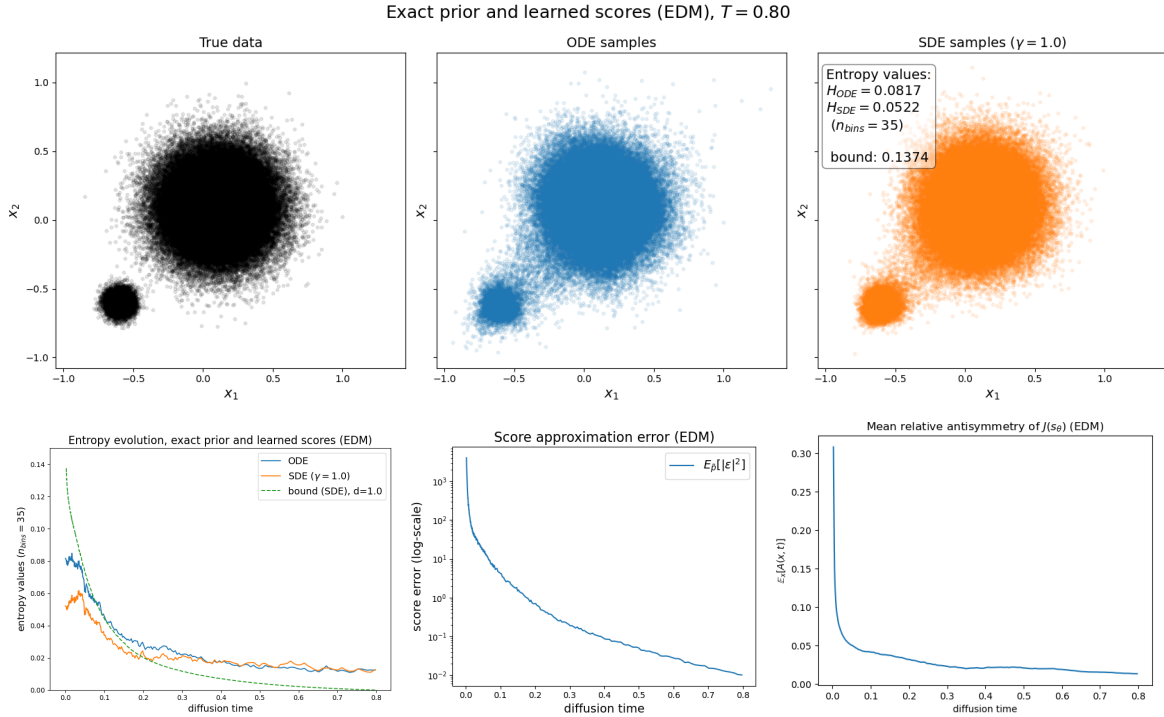


Figure 16: Generated distributions and entropy evolution for the EDM process, with exact prior and learned score functions for the 2D dataset. The two figures on the right show the score error and the relative antisymmetry of the score.